N71-30055

NASA TECHNICAL MEMORANDUM

NASA TM X-2305

NASA TM X-2305

CASE FILE COPY

LEWIS 9- BY 15-FOOT V/STOL WIND TUNNEL

by Joseph A. Yuska, James H. Diedrich, and Nestor Clough

Lewis Research Center
Cleveland, Ohio 44135

NATIONAL AERONAUTICS AND SPACE ADMINISTRATION • WASHINGTON, D. C. • JULY 1971

1. Report No.	2. Government Accession No.	3. Recipient's Catalog No.
NASA TM X-2305		

4. Title and Subtitle	5. Report Date
LEWIS 9- BY 15-FOOT V/STOL WIND TUNNEL	July 1971
	6. Performing Organization Code
7. Author(s)	8. Performing Organization Report No.
Joseph A. Yuska, James H. Diedrich, and Nestor Clough	E-6055
9. Performing Organization Name and Address	10. Work Unit No.
Lewis Research Center National Aeronautics and Space Administration Cleveland, Ohio 44135	721-56
	11. Contract or Grant No.
12. Sponsoring Agency Name and Address	13. Type of Report and Period Covered
National Aeronautics and Space Administration Washington, D.C. 20546	Technical Memorandum
	14. Sponsoring Agency Code

15. Supplementary Notes

16. Abstract

A 9- by 15-Foot V/STOL Wind Tunnel was built in the return leg of the 8- by 6-Foot Supersonic Wind Tunnel at the NASA Lewis Research Center. The test section has a velocity range of 13.4 to 78.2 meters per second (30 to 175 mph). This report describes the features of the wind tunnel and presents the results of the initial calibration in sufficient detail to guide prospective users in designing experiments. The methods used to design the tunnel inlet section, the test-section wall slot geometry, and the diffuser section are described in detail in separate appendixes.

17. Key Words (Suggested by Author(s))		18. Distribution Statement
V/STOL	Boundary layer	Unclassified - unlimited
Wind tunnel	Calibration	
Diffuser	Turbulence	
Inlet		

19. Security Classif. (of this report)	20. Security Classif. (of this page)	21. No. of Pages	22. Price*
Unclassified	Unclassified	48	$3.00

*For sale by the National Technical Information Service, Springfield, Virginia 22151

LEWIS 9- BY 15-FOOT V/STOL WIND TUNNEL

by Joseph A. Yuska, James H. Diedrich, and Nestor Clough

Lewis Research Center

SUMMARY

A 9- by 15-Foot V/STOL Wind Tunnel was built in the return leg of the 8- by 6-Foot Supersonic Wind Tunnel at the NASA Lewis Research Center. The test section has a velocity range of 13.4 to 78.2 meters per second (30 to 175 mph). This report describes the features of the wind tunnel and presents the results of the initial calibration in sufficient detail to guide prospective users in designing experiments. The methods used to design the tunnel inlet section, the test-section wall slot geometry, and the diffuser section are described in detail in separate appendixes.

INTRODUCTION

Analysis of propulsion requirements for vertical-takeoff-and-landing (VTOL) aircraft has uncovered several problem areas requiring experimental investigation. One of the problems is the effect of crossflow velocities on the performance of the thrusting systems. Crossflow velocities occur during transition flight, when the aircraft is moving from hover to horizontal flight or the reverse. For most VTOL aircraft with vertically mounted lift engines or lift fans, the air must turn approximately 90° into the inlet. In addition, the performance of the thrustor is more dependent on the interaction of the airframe and propulsion system than it is for conventional aircraft. The thrustor system also produces induced forces on the aircraft aerodynamic surfaces. The induced forces can be either helpful or detrimental to the overall aircraft performance. Therefore, there is a requirement to test the thrustor system in its installed condition to obtain valid thrustor performance data.

In order to investigate these problems experimentally, a subsonic facility was required to provide crossflow velocities. The facility had to be capable of developing velocicites from a minimum for short-takeoff-and-landing (STOL) testing (i.e., approx. 13.4 m/sec, or 30 mph) to typical values at conversion for vertical-takeoff-and-landing (VTOL)

testing (i.e., approx. 78.2 m/sec, or 175 mph). The facility had to be large enough to accommodate models with thrustors having large jet efflux. After a survey of existing facilities at the Lewis Research Center, the desired test section was built in the return leg of the 8- by 6-Foot Supersonic Wind Tunnel. The final dimensions of the V/STOL test section were determined from the available maximum weight flow and the desired maximum velocity.

This report is intended to serve three purposes: (1) to present the design considerations and auxiliary facilities for the test section, (2) to present the results of the calibration of the test section, and (3) to serve as a guide to prospective users in designing experiments for the wind tunnel. The report covers the description of the facility, the test-section airflow characteristics, the balance system, facility services, and the instrumentation and data processing services. The methods used to design the inlet section, the test-section wall openings, and the diffuser section are covered in detail in separate appendixes.

GENERAL DESCRIPTION

Figure 1 shows the overall view of the V/STOL test facility located in the return leg of the 8- by 6-Foot Supersonic Wind Tunnel. The V/STOL test facility consists of the following components, shown in figure 2: (1) entrance flow control section, (2) cooler (flow straightener), (3) settling section, (4) inlet contraction, (5) test section, (6) diffuser, and (7) exit. The inside dimensions of the return leg of the 8- by 6-Foot Supersonic Wind Tunnel are 10.70 meters by 9.15 meters (35 ft by 30 ft) at station 0, and 9.15 meters by 9.15 meters (30 ft by 30 ft) at station 236.

The flow control section contains two 6.7- by 3.8-meter (22- by 12.5-ft) sliding steel doors which are used to vary the velocity in the test section. The cooler is a finned-tube water heat exchanger. The cooler is used to control the inlet temperature to the drive compressor. Consequently, the temperature in the V/STOL test section remains essentially steady at a particular test condition. However, the cooler is not intended to control the temperature about a predetermined level. The cooler also serves to straighten the flow in the return leg of the tunnel.

The finned tubes are approximately 38 millimeters (1.5 in.) in outside diameter, and are the major source of turbulence in the V/STOL test section. The settling chamber is 24.6 meters (80.5 ft) long (650 cooler tube diameters), which tends to damp out most of the turbulence from the cooler. A piezometer ring is located in the settling chamber at station 0 and is used to measure the static pressure in the settling chamber.

The inlet was designed to provide constant axial acceleration of the tunnel airstream. Inlet design considerations and details are presented in appendix A. The area contraction ratio of the inlet is 8:1. The test section is 8.75 meters (28.667 ft) long. The walls

have been diverged slightly to account for longitudinal boundary-layer buildup. The cross-sectional dimensions are 2.72 meters by 4.58 meters (9 ft by 15 ft) at station 27.7, and 2.72 meters by 4.65 meters (9 ft by 15.25 ft) at station 56.3. The ceiling and floor are completely closed. The side walls are 11 percent open, provided by four 102-millimeter (4-in.) slots running the entire length of the test section, as shown in figure 3. The walls are slotted to reduce tunnel wall interference to a minimum when testing VTOL models. Details of the wall slot design are given in appendix B. The ceiling and wall panels are bolted to the tunnel structure. This construction technique permits changes in slot geometry. There are four plexiglass windows in the walls and one in the ceiling that are used to allow illumination of the test section and to view the model through closed-circuit television.

The diffuser is 20.75 meters (68 ft) long and has an included angle of 6.8°. The cross-section dimensions are 5.19 meters (17 ft) high by 7.09 meters (23.25 ft) wide at station 124.3. Diffuser design considerations and details are presented in appendix C. Bulkhead seals at station 0 and station 124.3 prevent airflow through the duct area around the test section. The space surrounding the test section is at the same static pressure as the test section. Access beneath the test section is provided by a 2.08- by 2.08-meter (6.8- by 6.8-ft) doorway at the diffuser bulkhead and by a personnel doorway through the outside concrete wall.

TEST-SECTION AIRFLOW CHARACTERISTICS

The airflow characteristics of most concern to the test planner are velocity range, dynamic pressure uniformity, longitudinal static-pressure variation, and turbulence level. In order to measure these variables, three instrumented rakes were installed in the test section at three longitudinal stations: 27.7 (forward); 40.6 (middle); and 52.6 (aft). Figure 4 shows a typical rake installation at one longitudinal station. Mounted on each rake were five pitot-static probes, one thermocouple probe (except rake 2 which had two thermocouple probes), and one hot-wire anemometer probe. The details of these probes are shown in figure 5. Two piezometer rings with 12 interconnected taps on each ring were located permanently at station 0 and at station 27.7.

It should be noted that the test-section walls and ceiling were 40 percent open (basic tunnel structure) when the airflow characteristics were measured. Since then the ceiling has been completely closed and the wall opening reduced to 11 percent (fig. 3).

Velocity Range

The test-section dynamic pressure is set by a combination of the drive compressor

weight flow and the position of the flow control doors. The differential pressure between the two piezometer rings was measured and correlated to the average of the dynamic pressures measured by the 15 pitot-static probes. This correlation was made at each of three longitudinal stations: 27.7 (forward); 40.6 (middle); and 52.6 (aft). Results are shown in figure 6.

The corresponding velocity range obtained in the test section at the midposition is shown in figure 7. With the drive compressor set at its rated speed, the test-section velocity can be varied from 76.1 meters per second (170.6 mph) to 22.3 meters per second (49.9 mph) by varying the position of the flow control doors from closed to fully open. With the flow control doors fully open, the test-section velocity can be reduced to 13.4 meters per second (30 mph) by reducing the drive compressor speed to its minimum controlled speed.

The data presented in figure 7 are for an empty test section. For normal test conditions, the maximum velocity in the test section will be reduced by the blockage introduced by the particular model and is also limited by the allowable differential pressure across the outside walls of the supersonic diffuser discharge section (fig. 1).

It is necessary to limit the internal air pressure in the diffuser discharge section (fig. 1) to a value of 3610-N/m^2 (75.5-lb/ft^2) pressure difference in order not to exceed the stress limits of the walls. Since ambient pressure is established in the region of the inlet doors where makeup air is introduced (fig. 1), any increase in pressure drop through the V/STOL tunnel will increase the pressure at the diffuser discharge section. Thus, any proposed model installation or modification to the V/STOL tunnel (or to any part of the tunnel circuit upstream of the inlet doors) should be carefully examined for effect on diffuser section pressure. Any increase in pressure drop through the V/STOL tunnel will require a reduction in maximum test-section velocity to maintain the allowable pressure differential at the diffuser discharge section.

Experience with the wing installation of figure 3 has shown that, for a model frontal area of 5 percent of the test-section cross-sectional area, the maximum obtainable velocity was 72.4 meters per second (162 mph); and with a model frontal area of 7.8 percent of the test-section cross-sectional area, the maximum obtainable velocity was 68.3 meters per second (153 mph).

Dynamic Pressure Uniformity

Figure 8 shows the dynamic pressure variation at the midposition (station 40.6) of the test section. The dynamic pressure variation is expressed as a ratio $q/\bar{q}$, where q is the local value of dynamic pressure and $\bar{q}$ is the average dynamic pressure of all the readings at a given rake location in the test section. Ninety-seven percent of the data fall within the ±2-percent band of the average dynamic pressure, as shown.

Static-Pressure Variation

The average test-section static pressure at three longitudinal stations is plotted in figure 9. There is no longitudinal static-pressure gradient below a $\bar{q}$ of 263 N/m^2 (55 lb/ft^2). Above a $\bar{q}$ of 263 N/m^2 (55 lb/ft^2) the static pressure at station 52.6 tends to be about 0.1 percent higher than at stations 27.7 and 40.6.

Turbulence Measurement

The free-stream turbulence in the test section was measured with a hot-wire anemometer mounted on each of the three survey rakes in the position shown in figure 4. It was assumed that the turbulence was isotropic; hence, no efforts were made to measure individual turbulence components. The probes were oriented with the sensing wire element horizontal (parallel to the lateral axis) and normal to the tunnel airflow, as shown in figure 10. The orientation of the probe as shown is sensitive to fluctuating components in the vertical-longitudinal plane and in the vertical-lateral plane and is insensitive to fluctuations in the lateral-longitudinal plane.

Root-mean-square turbulence level. - In the following discussion, the percent turbulence is defined as:

$$\text{Percent turbulence} = \frac{\text{Magnitude of fluctuating velocity component}}{\text{Magnitude of free-stream velocity}}$$

Percent turbulence values are plotted against tunnel dynamic pressure in figures 11(a) to (c). These figures show data for each probe at the forward, middle, and aft rake survey stations in the test section. There was no uniform trend of the turbulence data with the tunnel dynamic pressure. There were, however, higher turbulence levels at the highest dynamic pressure values. The rms values were computed for each survey station and for each hot-wire probe. These values are plotted along the right edge of the figures. The rms values had a consistent trend at each survey station; for example, the center probe on rake 2 indicated the lowest turbulence level, while the probes on the rakes on either side indicated significantly higher turbulence levels. Also, the probe on the rake adjacent to the inside wall (rake 1) indicated higher turbulence levels than the probe on the rake adjacent to the outside wall (rake 3).

After the first model was installed, the test-section ceiling was completely closed, and the wall slot openings were reduced to 11 percent open (fig. 3). Rake 1 was reinstalled at the midposition, and turbulence measurements were repeated. The results (fig. 12) show that the turbulence level was decreased with the reduced slot opening.

Turbulence factor. - The principal effect of turbulence on measurements made in wind tunnels is to cause the boundary-layer development on test surfaces to depart from the development occurring in free air. Drag measurements are affected most by this phenomenon. The simplest method of accounting for the presence of wind tunnel turbulence is to compute an "effective" Reynolds number to relate the test data to free-air conditions. The method proposed by reference 1 is

$$\text{Effective Reynolds number} = (\text{Turbulence factor}) \times (\text{Test Reynolds number})$$

The turbulence factor is a function of the overall turbulence level. In the V/STOL tunnel, the turbulence level also varies from point to point within the test section. At the center of the test section the rms turbulence level was about 0.75 percent. For this representative value, the turbulence factor is 1.6 from figure 3:34 of reference 1. According to reference 1, a value of 1.4 or lower is considered desirable for reliable drag measurements. Reductions in turbulence level can be accomplished by installing damping screens in the settling section of the tunnel. However, the additional pressure drop of the damping screens would cause a reduction in the maximum test-section velocity due to the backpressure effect on the supersonic tunnel diffuser discharge section. At present, damping screens have not been installed.

Wall Boundary Layer

The boundary layer on the tunnel floor at a distance of 158 millimeters (6.2 in.) downstream of the entrance to the test section was measured using the rake shown in figure 13. The rake had 13 total-pressure probes and one static-pressure probe. The measured total-pressure probe locations from the tunnel floor were as shown in figure 14. The static-pressure probe is located approximately 114 millimeters (4.5 in.) from the floor.

The air velocities at each probe location were determined from the absolute total- and static-pressure measurements. Figure 15 shows four sets of reduced data in which probe location above the floor is plotted against the local velocity. The data cover the range of test conditions from minimum to maximum tunnel velocity with two intermediate points, and are typical of the results obtained.

The boundary-layer thickness δ, as shown in figure 15, was taken at a value of local velocity V equal to 0.995 the free-stream velocity V_0. The figure indicates that the total boundary-layer thickness at the measuring station is about 47 millimeters (1.85 in.) from minimum to maximum tunnel velocity.

These data were found to be represented by the standard, flat-plate, boundary-layer equation

$$\frac{V}{V_0} = \left(\frac{y}{\delta}\right)^{1/n} \tag{1}$$

where y is the boundary-layer dimension. The value of the exponent n was determined to be 6.45 over the range of tunnel velocities tested. Since the value of n in equation (1) was found to be approximately constant with varying tunnel velocity V_0, the ratio of displacement thickness δ^* to boundary-layer thickness δ is a constant (ref. 2) given by

$$\frac{\delta^*}{\delta} = \frac{1}{n+1} \tag{2}$$

The displacement thickness δ^* calculated from equation (2) with $n = 6.45$ is also plotted in figure 15. The displacement thickness is about 6.3 millimeters (0.248 in.) from minimum to maximum tunnel velocity.

The growth of the boundary layer along the floor of the wind tunnel was calculated by assuming fully turbulent flow. Since the measured exponent n in equation (1) was not far removed from the value of 7.0, the classical equation for boundary-layer growth along a smooth flat plate, as given in reference 2, was used:

$$\delta = 0.37\, X'\left(\frac{V_0 X'}{\nu}\right)^{-1/5} \tag{3}$$

where X' is the distance down the plate measured from the point of zero boundary-layer thickness and ν is the kinematic viscosity.

To use equation (3), the virtual origin for the boundary layer was determined by using the measured value of boundary-layer thickness presented herein. Equation (3) can be written as

$$X_0 = \left(\frac{\delta_0}{0.37}\right)^{5/4}\left(\frac{V_0}{\nu}\right)^{1/4} \tag{4}$$

where X_0 is the distance from the measured boundary layer to the point where the boundary layer would be zero (virtual origin), and δ_0 is the measured boundary layer. Equation (3) is then modified to

$$\delta = 0.37\left(\frac{\nu}{V_0}\right)^{1/5}(X + X_0)^{4/5} \tag{5}$$

where X is the distance down the tunnel measured from the rake position, and X_0 is the distance to the virtual origin.

The growth of the boundary layer along the floor from the probe position was calculated using equations (4) and (5) for the maximum tunnel velocity tested. The average tunnel air temperature was 560° R. The results are shown in figure 16(a). The total boundary-layer thickness at the exit of the test section is seen to be about 127 millimeters (5.0 in.). The displacement thickness δ^* was calculated for the same conditions by using equation (2) with $n = 6.45$. The results are shown in figure 16(b). The displacement thickness at the test-section exit is seen to be about 17.3 millimeters (0.68 in.).

Assuming the boundary layer grows at the same rate along the ceiling and side walls as along the floor, an effective area blockage due to the boundary-layer growth can be calculated. The displacement boundary-layer thickness grows from about 5.1 millimeters (0.2 in.) to about 17.3 millimeters (0.68 in.) from test-section inlet to test-section exit. This growth of about 12.2 millimeters (0.48 in.) represents a blocked area of about 0.214 square meter (2.0 ft^2). The test-section side walls were diverged 382 millimeters (1.5 in.) to account for this blocked area. The test-section exit area is 0.209 square meter (2.25 ft^2) greater than the inlet area. Therefore, the effective blocked area due to the boundary-layer growth is minimized, as indicated in figure 9.

The preceding discussion on effective blocked area does not take into account the slotted walls and their effect on the boundary layer. This effect is unknown, and no attempt has been made to account for it.

BALANCE SYSTEM

The test facility does not have a standard balance system. Each model using the test facility must have its own balance system. For example, the balance system for the first VTOL fan-in-wing model (fig. 3) was supported from the test section structure. Supporting the balance from the tunnel produced fluctuating load-cell readings due to wing and tunnel vibrations. For balance systems of this type, electrical filters must be used to provide a signal representative of the mean value.

SERVICE SYSTEMS

Air Systems

Drive air. - Drive air can be supplied from two separate systems. One has a fixed capacity and the other is capable of continuous flow.

The fixed-capacity system has a volume of 60 cubic meters (1976 ft^3) and can be pressurized to 20.6×10^6 N/m^2 (3000 psig). The delivery pressure can be set at a prescribed value with a pressure regulator. The piping connecting the high-pressure reservoir to the test section was designed for a flow rate of 6.8 kilograms per second (15 lb/sec) at a delivery pressure of 10.3×10^6 N/m^2 (1500 psig). The flow rate is measured with a calibrated flat-plate orifice.

The drive-air temperature can be heated and controlled to a maximum of 367 K (660° R). A shell-and-tube counterflow heat exchanger is used. The dew point of the air is 244 K (440° R) at standard conditions. The available test time using this system is dependent on the pressure level and flow rate of the machine under test, as shown in figure 17. For a 10.3×10^6-N/m^2 (1500-psig), 3.6-kilogram-per-second (8-lb/sec) flow rate, the available test time is about 30 minutes. Approximately 8 hours are required to recharge the system to 20.6×10^6 N/m^2 (3000 psig) after a 30-minute run.

The continuous-flow system can simultaneously deliver air to the test section through two piping systems. The first was designed for a flow rate of 4.5 kilograms per second (10 lb/sec) at 25×10^5 N/m^2 (350 psig) at ambient temperature. The second passes through a secondary line in the heat exchanger and was designed for a flow rate of 0.45 kilogram per second (1 lb/sec) at 8.7×10^5 N/m^2 (125 psig) at a temperature of 367 K (660° R).

Service air. - Service air at 8.7×10^5 N/m^2 (125 psig) is supplied at 0.23 kilogram per second (0.5 lb/sec) for power tools.

Lubrication Systems

Oil. - The lubrication oil system can supply oil at 2.3 kilograms per minute (5 lb/min) and scavenge at 6.8 kilograms per minute (15 lb/min). The oil used in the VTOL drive turbine conformed to MIL-L-7808.

Freon and trichloroethylene. - The first test model contained a high-speed slipring that required cooling and lubrication. For this model, trichloroethylene was the best lubricant. This system delivers trichloroethylene at 15 liters per hour (4 gal/hr) to the model and also contains provisions for a freon TF purge at the same rate to flush the residual trichloroethylene from the system.

Gaseous Nitrogen System

A 15.2×10^6-N/m^2 (2200-psig) gaseous nitrogen supply at various regulated pressures is used for the model control systems.

Electrical Power

The following types of electrical power are available at the test section:

(1) 480-volt, 60-cycle alternating current; three phase
(2) 208-volt, 60-cycle alternating current; three phase
(3) 120-volt, 60-cycle alternating current; one phase
(4) 28-volt direct current

Hydraulic Power

A hydraulic pumping unit capable of pumping up to 15 liters per minute (4 gal/min) at 20.6×10^6 N/m^2 (3000 psig) is used for actuation of model system controls.

INSTRUMENTATION AND DATA RETRIEVAL

Control-Room Instrumentation

There are instruments in the control room for observing model performance and tunnel conditions. The tunnel static and dynamic pressures are displayed on digital readout voltmeters, and tunnel temperature is indicated on a panel meter. The model and test section can be viewed on two closed-circuit television monitors.

Model forces, individual readings or the summation of load-cell readings, can be displayed on digital readout. Transient loads can be recorded on a recording galvanometer or on magnetic tape. Some model pressures and temperatures can be displayed on meter readouts and/or a recording galvanometer.

For models having rotating parts, the rotational speed can be digitally displayed. The model vibrations can be monitored with audio and visual warning signals activated for high levels of vibration.

Automatic Recording Equipment

The Lewis Research Center has a central recording system called the Central Automatic Digital Data Encoder (CADDE) that is used by many of the test facilities to record digital readings from transducers of pressure, voltage, and events per unit time. The system has a 500-data-word capacity. Reference 3 gives a detailed description of the system. The data are recorded on magnetic tape as binary-coded decimal digits with additional characters for identification and computation instructions. The magnetic tape is the permanent record of the raw data. In addition, the data may be simultaneously recorded on an IBM 360 time-sharing computer system. This allows the test engineer to receive "on-line" computed data typed out in the control room after the data point is taken.

After recording, a duplicated tape is made to process the data as a stored program on an IBM 7094 computer.

Analog Computer

Selected model parameters can be input to an analog computer located beneath the control room. The computed analog data can be displayed on X-Y plotters in the control room to provide the test engineer with real-time data.

Model Instrumentation

Instrumentation leads from the model are terminated at patch panels located on top of and below the test section. Each panel has permanent connectors of various types as listed in table I. There are permanent cables between the patch panel and an auxiliary equipment room which contains the instrumentation power supplies, amplifiers, and readout equipment. There are 110 strain-gage balance panels which are used for strain-gage-pressure and load-cell transducers. A pressure multiplexing system (Scanivalve) capable of controlling five scanivalves is available. This system increases the number of model pressures that can be measured on one transducer, provided that the 500-data-word limit of the CADDE system is not exceeded.

Lewis Research Center,
National Aeronautics and Space Administration,
Cleveland, Ohio, March 11, 1971,
721-56.

APPENDIX A

DESIGN OF THE INLET CONTRACTION

If the curvature of the wind tunnel inlet is such that large local velocity gradients are present, it is unlikely that a uniform distribution will be obtained in the test section. In general, the inlet should be faired out gradually at the downstream end (continually decreasing curvature) so that local flow velocity changes are small near the test section. Furthermore, in order to avoid flow discontinuities in the corners of the inlet, the flow velocities on the walls of the inlet should be the same at equal axial distances down the contraction. To do this the curvature of all four walls must be the same at equal axial distances, or in other words, the change in wall ordinate should be the same for all four walls (i.e., identical profiles).

The NASA low-speed wind tunnels (Ames 40 by 80 Foot, Langley 7 by 10 Foot and 30 by 60 Foot, and Lewis Icing Research Tunnel (IRT) and Altitude Wind Tunnel (AWT)) have a long history of acceptable performance. All the wind tunnels cited have inlets of the modified constant-axial-acceleration type. The term "modified constant acceleration" refers to constant axial acceleration modified to meet the requirements of zero acceleration at the entrance to the test section and zero acceleration at the entrance to the inlet.

A wind tunnel inlet with wall contours that produce constant axial acceleration has the undesirable feature of discontinuous velocities at both entrance and exit. The reason for these discontinuities is the step change in acceleration from zero to some positive value at the entrance and back down to zero at the exit. To remove the discontinuity at the entrance to the inlet, a straight-line transition section is employed tangent to the constant-acceleration curve. From past experience at the various NASA centers, it has been determined that a 30° section provides the necessary transition from zero acceleration to some positive value with no adverse velocity gradients. To eliminate adverse velocity gradients at the exit of the contraction, and to gradually fair the inlet into the test section, an ellipse is fit tangent to the constant-acceleration curve and tangent to the test section at the point of the ellipse where its slope is zero.

The portions of the modified-constant-acceleration contraction inlet wall contour and its velocity and acceleration curves are diagrammed in figure 18. The total length of the inlet L, as shown in figure 18, is the sum of three sections (straight line, constant acceleration, and elliptical). The three sections are designed individually and then fit together. The procedure is to start with the constant-acceleration curve. The choice of the length of this section of the inlet ultimately determines the total length L. The ellipse and straight-line sections are then fitted to the constant-acceleration curve and

the overall length is determined. These steps are repeated as required to obtain the desired overall length.

This philosophy was employed in the design of the V/STOL tunnel inlet. The design method has never been published. Consequently, the detailed design procedure and the resulting design of the V/STOL tunnel inlet are presented herein.

Constant-Acceleration Section

The constant-acceleration portion of the wall contours, as shown in figure 18, is designed by using the one-dimensional incompressible equation of continuity. Figure 19 is a schematic of the constant-acceleration curve and the coordinate system used. The areas at the entrance to the inlet and at the test section are A_U and A_T, respectively. (Inlet contraction ratio is A_U/A_T.) The length of the constant-acceleration curve is L_a.

The wall coordinates of the constant-acceleration curve are determined as follows (fig. 19): For constant axial acceleration

$$\frac{dV}{dt} = V\frac{dV}{dx_a} = \text{Constant} \tag{A1}$$

where

V axial velocity

x_a axial distance from origin

t time

Solving equation (A1) for V yields

$$V = (ax_a + b)^{1/2} \tag{A2}$$

The continuity boundary conditions at the entrance and the exit of the constant-acceleration curve are

$$\left.\begin{aligned} V &= \frac{\dot{\omega}}{\rho A_U} \quad \text{at } x_a = 0 \\ &\text{and} \\ V &= \frac{\dot{\omega}}{\rho A_T} \quad \text{at } x_a = L_a \end{aligned}\right\} \tag{A3}$$

where

$\dot{\omega}$ weight flow rate

ρ density (constant with x_a)

With these boundary conditions, equation (A2) becomes

$$V = \frac{\dot{\omega}}{\rho}\left[\left(\frac{1}{A_T^2} - \frac{1}{A_U^2}\right)\frac{x_a}{L_a} + \frac{1}{A_U^2}\right]^{1/2} \tag{A4}$$

As mentioned previously, the flow velocities on the four walls of the inlet should be the same at equal axial distance down the contraction. To do this requires that the curvature of all four walls be the same at equal axial distances. This is done by keeping the change in wall ordinates the same for all four walls, which is the same as keeping a constant difference δ in ordinates between top wall dimension and side wall dimension. Consequently, only one wall is designed and the remaining walls are derived from the designed wall.

With a constant difference δ between ordinates of the side walls and the top walls, the cross-sectional area is

$$A = 2y_a(2y_a + \delta) \tag{A5}$$

Thus, from equation (A5) and continuity,

$$\frac{\dot{\omega}}{\rho}\frac{1}{V} = 2y_a(2y_a + \delta) \tag{A6}$$

Substituting equation (A6) into equation (A4) yields

$$4y_a^2 + 2\delta y_a = \frac{1}{\left[\left(\frac{1}{A_T^2} - \frac{1}{A_U^2}\right)\frac{x_a}{L_a} + \frac{1}{A_U^2}\right]^{1/2}} \tag{A7}$$

In terms of wall coordinates with respect to the tunnel centerline and origin of the constant-acceleration curve as defined in figure 19,

$$y_a^2 + \frac{\delta}{2} y_a = \frac{\frac{1}{4}}{\left[\left(\frac{1}{A_T^2} - \frac{1}{A_U^2}\right)\frac{x_a}{L_a} + \frac{1}{A_U^2}\right]^{1/2}} \tag{A8}$$

Solution of equation (A8) will yield the x_a, y_a coordinates of the constant-acceleration curve shown in figure 19. The coordinates are seen to depend on the upstream and test-section areas (contraction ratio) and the particular length L_a. The value of δ can be determined from the test-section dimensions. For example, for a 2.74- by 4.58-meter (9- by 15-ft) test section, $\delta = 15 - 9 = 6$.

The length of the constant-acceleration curve L_a is somewhat arbitrary. It does, however, affect the overall length of the inlet section L and must be chosen by trial and error such that the overall length of the inlet is within the limits of good design. These design limits are such that if the cone is too long, cost increases and a significant boundary layer can build up; and if it is too short, steep velocity gradients will occur.

As a guide to the choice of the value of overall length L, data on inlet lengths for various wind tunnels were gathered. These data are shown in figure 20, in which the ratio of inlet to outlet hydraulic diameter is plotted as a function of total inlet length divided by inlet hydraulic diameter. The dashed curve divides the regions of good and poor flow. This is a theoretical curve developed in reference 4.

The tunnels to the left of the dashed curve are known to have relatively poor test-section flow in terms of nonuniform velocity profiles. The overall length of the inlet section L, as shown in figure 18, would include the contributions of the straight-line, elliptical, and constant-acceleration curves. Therefore, when using figure 20 as a guide in choosing L_a (the constant-acceleration-curve length), it is suggested that as an initial trial, L_a be made approximately equal to 1/3 L.

The differentiation of equation (A8) yields the slope of the constant-acceleration curve at any (x_a, y_a) point. This equation will be necessary in the subsequent discussion and is presented here for convenience.

$$m_a = \frac{dy_a}{dx_a} = \frac{-0.25}{2y_a + \frac{\delta}{2}} \frac{\frac{1}{2L_a}\left(\frac{1}{A_T^2} - \frac{1}{A_U^2}\right)}{\left[\left(\frac{1}{A_T^2} - \frac{1}{A_U^2}\right)\frac{x_a}{L_a} + \frac{1}{A_U^2}\right]^{3/2}} \tag{A9}$$

Straight-Line Section

The next step in the development of the inlet is to fit the straight-line section (fig. 18) to the constant-acceleration curve. The straight line is fit tangent to the constant-acceleration curve at the point X_1, as defined in figure 18. Figure 21 defines the coordinate system used in determining the point X_1.

The angle β of the straight-line section determines its slope. The problem is to determine the point on the constant-acceleration curve where this slope occurs. This is done by using equation (A9) with a slope set equal to $-\tan^{-1}\beta$; that is,

$$m_a = -\tan^{-1}\beta \tag{A10}$$

To determine the point $x_{a,1}$, $y_{a,1}$ (point on constant-acceleration curve whose slope is $\tan^{-1}\beta$), equations (A10), (A9), and (A8) are solved simultaneously for x_a, y_a.

The origin of the inlet can now be determined (i.e., $X = 0$, $Y = 0$) by extending the straight line from the tangent point $x_{a,1}$, $y_{a,1}$ to the intersection point with the upstream wall Y_u. The distance X_1 (fig. 21) is calculated from

$$X_1 = \frac{Y_u - y_{a,1}}{\tan \beta} \tag{A11}$$

Relative to the inlet origin, the coordinates at the tangent point X_1, Y_1 are then X_1 from equation (A11) with $Y_1 = y_{a,1}$.

Elliptical Section

The elliptical section, as shown in figure 18, must now be fit to the constant-acceleration curve. The geometry of the elliptical section is shown in figure 22. The point of tangency between the elliptical and the constant-acceleration curves must be prescribed in order to obtain a solution. The problem is to fit an ellipse tangent to the constant-acceleration curve at X_2, have a zero slope at the test section at X_3, and have a reasonable length $X_3 - X_2$.

The general equation of an ellipse with its center at its origin ($x_e = y_e = 0$, fig. 22) is

$$\left.\begin{aligned} &\frac{x_e^2}{a^2} + \frac{y_e^2}{b^2} = 1 \\ &\text{or} \\ &x_e = \pm\frac{a}{b}\left(b^2 - y_e^2\right)^{1/2} \end{aligned}\right\} \tag{A12}$$

As defined in figure 22, only the negative values of x_e and y_e are of interest. The slope of the ellipse in this quadrant is

$$m_e = \frac{dy_e}{dx_e} = \frac{-\left(b^2 - y_e^2\right)^{1/2}}{\left(\frac{a}{b}\right)y_e} \tag{A13}$$

Equation (A13) relates the slope of an ellipse with major and minor axes equal to a and b, respectively, to the y_e coordinate. The tangent point X_2 on the constant-acceleration curve is initially prescribed as $X_2 < (X_u + L_a)$. This defines the coordinates $x_{a,2}$, $y_{a,2}$, which are then used to calculate the slope of the constant-acceleration curve at this point by using equation (A9). This slope is set equal to the slope of the ellipse at $-x_{e,2}$, $-y_{e,2}$. Equation (A13) solved for $y_{e,2}$ becomes

$$y_{e,2} = -\frac{b^2}{\left(a^2 m_{e,2}^2 + b^2\right)^{1/2}} \tag{A14}$$

where $m_{e,2} = m_{a,2}$.

In general, the equation of an ellipse can also be written (from eq. (A12)) as

$$y_e = -b\sqrt{1 - \frac{x_e^2}{a^2}} \tag{A15}$$

and at $-y_{e,2}$, $-x_{e,2}$

$$y_{e,2} = -b\sqrt{1 - \frac{x_{e,2}^2}{a^2}} \tag{A16}$$

The length of the elliptical section $X_3 - X_2$ is then chosen such that L is within reasonable limits as discussed previously. From figure 22,

$$X_3 - X_2 = -x_{e,2} \tag{A17}$$

Then equations (A14) and (A16) represent two equations and three unknowns ($y_{e,2}$, b, and a). To determine these unknowns, another restriction must be placed on the ellipse. A particular restriction which simplifies the coordinate calculations and minimizes the ellipse size is proposed as follows: It can be shown that with $y_{e,2} = b/2.618$, the value of $x_{e,2}$ is minimum for any value of the slope at $x_{e,2}$, $y_{e,2}$. Therefore, let

$$y_{e,2} = kb \tag{A18}$$

By solving equations (A14), (A16), and (A18) simultaneously with a prescribed value of k, the values $y_{e,2}$, a, and b can be determined. With the determined values of a and b, the coordinate equation (eq. (A15)) can be solved for the ellipse.

In terms of the general inlet coordinate system defined in figure 18, the coordinate at the tangent point X_2 is

$$X_2 = X_1 + x_{a,2} - x_{a,1} \tag{A19}$$

and the X_3 coordinate is obtained from equation (A17), where $x_{e,2}$ was chosen as previously indicated. Values of L_a and $x_{e,2}$ are then adjusted as required to give the desired value of overall length L.

Finally, the coordinates of the elliptical section transformed to the general inlet origin are

$$Y = (b + Y_T) - b\sqrt{1 - \frac{(X_3 - X)^2}{a^2}} \tag{A20}$$

V/STOL Tunnel Inlet Contraction Design

The side walls of the V/STOL inlet contraction were chosen for the inlet design. The

test-section dimensions were 2.74 meters by 4.58 meters (9 ft by 15 ft), from which the side wall Y_T was determined to be 2.29 meters (7.5 ft). The test-section area A_T was 12.5 square meters (135 ft^2). The upstream entrance section dimensions were 9.1 meters by 9.6 meters (29.8 ft by 31.4 ft) for an area A_U = 87 square meters (935.7 ft^2). The value of Y_U for the side walls was 4.54 meters (14.9 ft).

With these inputs, the constant-acceleration-curve coordinates were determined from equation (A8) by choosing a value of L_a / 3.048 meters (10 ft). This yielded the coordinate equation

$$Y = y_a = \left[\frac{25}{(0.05372745031\, x_a + 0.0114211969)^{1/2}} + 2.25\right]^{1/2} + 1.5$$

where $0 \leq x_a \leq 10$. The straight-line section was fit to the constant-acceleration curve with a value of $\beta = 30^{\circ}$. The point of tangency was found at $x_{a,1}$ = 0.935 meter (3.06776 ft) and $y_{a,1}$ = 1.939 meters (6.3613 ft). From the ($x_{a,1}$, $y_{a,1}$) coordinates and by the previously described method, the inlet origin was determined, and a value of X_1 was determined to be 2.910 meters (9.550 ft) with Y_1 = 1.939 meters (6.3613 ft).

The point of tangency for the ellipse was prescribed at X_2 = 4.48 meters (14.740 ft), and the ellipse length was chosen as 2.135 meters (7.000 ft), so that X_3 = 6.32156 meters (20.740 ft). The coordinate equation for the elliptical section was then determined to be (using k = 1/2 in eq. (A17))

$$Y = 8.52463 - 1.02463\left[1 - 0.14506(20.740 - X)^2\right]$$

between the values of X_2 and X_3 of 4.493 and 6.322 meters (14.740 and 20.740 ft).

After the side-wall coordinates were calculated, the top- and bottom-wall ordinates were determined by subtracting the constant $\delta/2$ = 0.9 meter (3 ft) from each side-wall ordinate. Figure 23 shows the final design of the inlet contraction. The difference in length of the side walls and the top and bottom walls is due to the requirement of constant change in ordinate. The inside dimensions of the concrete structure in which the V/STOL tunnel is housed required the extension of the top and bottom walls as shown. Therefore, for the first 1.981 meters (6.500 ft) the inlet contraction is confined to the top and bottom walls only. After this a constant difference of $\delta/2$ = 0.9 meter (3 ft) in wall ordinates is maintained and the inlet becomes three dimensional.

The position of the V/STOL tunnel inlet contraction is plotted on figure 20 at a value of L/D_1^* of 0.89 and D_1^*/D_2^* of 2.72. The V/STOL inlet contraction is seen to fall very nearly on the theoretical dividing line between good and poor flow.

APPENDIX B

TUNNEL WALL SLOT DESIGN

In general, aerodynamic data obtained in wind tunnels are somewhat different than conditions in free air because of the effects introduced by the presence of the walls. This fact has been recognized for many years and the corrections for conventional wings are well known. The wall corrections for V/STOL models become complicated by the presence of the large wake angles and induced flows associated with powered or high-lift devices (ref. 5). Unlike conventional wings, the magnitudes of the corrections for V/STOL models are dependent on the wind tunnel velocity and the effective disk loading of the powered lift model. Confidence in the test data is enhanced if the correction is kept small or reduced to a negligible value. One method of achieving this objective is to vary the geometry of the tunnel walls by incorporating slots or perforations. The reason for this approach lies in the fact that wind tunnel corrections (usually expressed as a correction to the model angle of attack $\Delta\alpha$) are positive for a completely closed test section and negative for a completely open test section (free jet). Theoretically, some combination of open and closed walls or "mixed-boundaries" would result in a negligible correction configuration.

Considerable theory (refs. 6 to 9) and tests (refs. 10 and 11) are available for V/STOL aircraft models. In general, these references show that slots of 10 to 15 percent open are desirable to minimize interference effects. These results are based on test configurations where models are relatively small compared to test-section area.

For the V/STOL test section, there was some uncertainty in the slot design approach since the first model was a two-dimensional wing spanning the test section with a fan mounted in the center. Subsequent models would be different and there is no specific analytical method of determining the precise wall configuration for each model. The object therefore was to generally reduce the flow distortion around the fan rather than to determine a universal wall configuration that would yield a "zero-correction" tunnel for all models. Thus, mixed boundaries were designed for only the vertical walls of the V/STOL test section. The horizontal boundaries were left solid to facilitate the installation of the fan-in-wing test model and to maintain two-dimensionality.

The method used to calculate the slot dimensions for the vertical boundaries is described in reference 6. Figure 24 shows the arrangement of the model and test section, with tunnel rotated 90° to conform to conventional notation. Reference 6 analyzes the tunnel interference effects in terms of dimensionless slot parameters P_V for the vertical walls and P_H for the horizontal walls. Since the vertical walls are closed, $P_V = 0$ and only P_H is needed. Values of P_H against slot dimensions are shown in figure 24.

Desired values of P_H were determined from figure 25, which shows values of P_H

required to produce zero lift interference as a function of tunnel dimension ratio H/B with closed vertical walls. Also shown on the figure are points for zero blockage effect. From this figure, it was concluded that a value of $P_H = 0.87$ or larger was needed for the V/STOL section (H/B = 1.667).

Referring now to figure 24, values of the parameters L/H and A/L can be obtained corresponding to the desired value of P_H. For the V/STOL test section it was decided to use four slots in each of the horizontal walls. Other analyses and experience indicated this was a desirable number. As an initial trial, the following values were chosen:

A = 0.076 m (3 in.)
L = 0.56 m (22 in.)

Then,

A/L = 3/22 = 0.136
L/H = 22/7.5 × 10 = 0.245

From figure 24 these values correspond to $P_H = 0.895$, which is slightly greater than the theoretical value indicated in figure 25. Experimental data from reference 6 indicate that values of P_H slightly larger than theoretical are required to accomplish zero-lift-interference conditions. Consequently, the preceding slot parameters were used.

Referring to figure 24, the wall open-area ratio is computed as

$$\text{Open-area ratio} = \frac{\text{Slot area}}{\text{Wall area}} = \frac{NA}{2B}$$

For the configuration selected,

$$\text{Open-area ratio} = \frac{4(3)}{108} = 0.11$$

Thus, the slotted walls are 11 percent open. The existing walls were covered with plywood, incorporating the slots in the locations specified previously. The slot width A was increased to 0.101 meter (4.0 in.) to compensate for the blocked slot area due to vertical structural members.

APPENDIX C

DESIGN OF THE DIFFUSER SECTION

In general, wind tunnel diffusers are designed to provide for minimum total-pressure loss and maximum static-pressure recovery. Total-pressure loss in a wind tunnel diffuser occurs because of wall friction and flow separation from the diffuser walls. In the V/STOL wind tunnel, a third source of total-pressure loss is present. This is the "dump loss" due to the sudden expansion from the diffuser exit area to the concrete structure area. The V/STOL diffuser configuration is illustrated in figure 26.

The V/STOL tunnel diffuser was designed to minimize the total-pressure loss in order to minimize the increase in backpressure on the supersonic diffuser discharge section (fig. 1). Cost considerations were also important, so a minimum-length diffuser was desired. The diffuser design for the V/STOL tunnel is the result of a compromise between minimum total-pressure loss and minimum cost (i.e., minimum length).

The variables affecting the performance of conical, rectangular, or two-dimensional diffusers are area ratio, length, included diffuser angle, and inlet boundary-layer thickness. For a diffuser, the selection of any two of the geometric variables (length, area ratio, or angle) fixes the third. The inlet boundary-layer thickness is, in most cases, an uncontrolled variable.

For a fixed inlet boundary-layer thickness and area ratio, a set of typical performance curves as a function of included diffuser angle 2θ appears as shown in figure 27. The diffuser performance is expressed in terms of the two pressure coefficient curves shown. The upper curve is the diffuser static-pressure-recovery coefficient, defined as $(p_2 - p_1)/\bar{q}_1$ where p_2 is the exit static pressure, p_1 the inlet static pressure, and $\bar{q}_1$ the inlet average dynamic pressure. The lower curve is the diffuser total-pressure-loss coefficient defined as $(\bar{P}_1 - \bar{P}_2)/\bar{q}_1$ where $\bar{P}_1$ and $\bar{P}_2$ are the inlet and exit average total pressure, respectively. Point "a" represents the angle at which the diffuser begins to stall; that is, the flow separates somewhere within the diffuser. Point "b" represents the angle at which "appreciable" stall occurs. For angles greater than that at point "b", the diffuser performance is generally unsteady and will cause flow unsteadiness in the test section itself. The points of maximum static-pressure recovery and minimum total-pressure loss, which generally occur after the diffuser begins to stall, represent the angle for which the average discharge dynamic head $\bar{q}_2$ will be very close to its minimum value.

The angle at which the "optimum" diffuser performance is obtained is chosen at either the points of maximum static-pressure recovery or the point of minimum total-pressure loss, depending on the criterion of optimization.

For a fixed inlet boundary-layer thickness and included diffuser angle, the total-

pressure loss increases with increasing area ratio. This increase in total-pressure loss is primarily due to friction loss, since increasing the area ratio with a constant included angle increases the diffuser length. For a standard wind tunnel diffuser, curves could be developed for total-pressure loss as a function of area ratio for fixed values of 2θ. These curves would serve as a guide in the selection of a value of included diffuser angle 2θ and diffuser area ratio A_2/A_1.

As mentioned previously, the V/STOL diffuser included another source of total-pressure loss, the dump loss. In this design, the overall total-pressure loss, from the diffuser inlet to the area in which the diffuser exit flow is discharged, was to be minimized to reduce the backpressure on the supersonic diffuser discharge section (fig. 1). Since the average exit discharge dynamic pressure of the diffuser would decrease with increasing area ratio, the "dump" loss would decrease with increasing area ratio A_2/A_1. Then, since the dump loss decreases and the diffuser loss increases with area ratio, for a fixed value of inlet boundary-layer thickness, there is in principle a particular value of the area ratio A_2/A_1 and the included angle 2θ which will yield a minimum loss in total pressure.

To design the V/STOL diffuser using the preceding approach of minimizing overall total-pressure loss and cost, data from references 12 and 13 were used. Most available diffuser performance data were for two-dimensional or conical diffusers, while the proposed diffuser was a three-dimensional rectangular type. A comparison of results of two-dimensional and conical diffusers is shown in figure 28 for a diffuser with an area ratio of 3.0 and nearly equal inlet boundary-layer-thickness parameters $2\delta^*/D_1$ where δ^* is displacement thickness, and D_1 is hydraulic diameter of the diffuser at its entrance. The performance of the two types of diffusers is virtually identical, justifying the use of either type of diffuser data to represent the other.

To determine if these data can be used to predict the performance for three-dimensional rectangular diffusers, experimental performance points for the Lewis Research Center Icing Research Tunnel (IRT) were employed. The IRT diffuser is a three-dimensional, rectangular type similar to the configuration for the V/STOL wind tunnel. Figure 29 shows a comparison of two-dimensional results from references 12 and 13 with the experimental points from the IRT diffuser obtained at two axial positions. The curves on the figure were interpolated from the results presented in references 12 and 13 to arrive at curves for area ratios corresponding to the IRT experimental results (A_2/A_1 = 3.61 and 2.48). The boundary-layer profile at the entrance to the diffuser was determined experimentally. The displacement thickness was then calculated, and the value of $2\delta^*/D_1$ was determined to be about 0.010. The results in figure 29 indicate a good agreement between the two- and three-dimensional results, confirming the use of two-dimensional data for design of the V/STOL diffuser.

The displacement thickness at the entrance to the V/STOL diffuser was initially estimated to be about 185 millimeters (0.73 in.). This value is close to that calculated

from the experimentally determined thickness at the entrance to the test section as reported in the main body of the report. The hydraulic diameter of the diffuser inlet is about 3.3 meters (11 ft); therefore, the boundary-layer parameter is $2\delta^*/D_1 = 0.011$.

Two-dimensional static-pressure-recovery curves for $2\delta^*/D_1 = 0.010$ and for a range of area ratios were available from reference 12. These curves are shown in figure 30. The value of 2θ for minimum total-pressure loss varies from around 6.5° to 7° for the data shown.

By assuming one-dimensional incompressible flow, it is possible to relate the average total-pressure loss of a diffuser to its static-pressure-recovery performance. The total pressure at the diffuser exit is (fig. 26)

$$\overline{P}_2 = p_2 + \frac{1}{2}\rho\overline{V}_2^2 \tag{C1}$$

where ρ is air density. From continuity,

$$\overline{V}_2 = \overline{V}_1\left(\frac{A_1}{A_2}\right) \tag{C2}$$

Then, combining equations (C1) and (C2)

$$\overline{P}_2 = p_2 + \frac{1}{2}\rho\overline{V}_1^2\left(\frac{A_1}{A_2}\right)^2 \tag{C3}$$

Also, at the diffuser inlet

$$\overline{P}_1 = p_1 + \frac{1}{2}\rho\overline{V}_1^2 \tag{C4}$$

Subtracting equation (C3) from equation (C4) and rearranging yields

$$\frac{\overline{P}_1 - \overline{P}_2}{\overline{q}_1} = \left[1 - \left(\frac{A_1}{A_2}\right)^2\right] - \left(\frac{p_2 - p_1}{\overline{q}_1}\right) \tag{C5}$$

where

$$\bar{q}_1 = \frac{1}{2}\rho\bar{V}_1^2$$

Equation (C5) defines the one-dimensional incompressible total-pressure loss of the diffusing section alone. For the sudden expansion type of diffusion, a second source of total-pressure loss is present. The discharge jet dump loss can be calculated as follows:

From figure 26

$$\frac{\bar{P}_1 - \bar{P}_e}{\bar{q}_1} = \frac{\bar{P}_1 - \bar{P}_2}{\bar{q}_1} + \frac{\bar{P}_2 - \bar{P}_e}{\bar{q}_1} \tag{C6}$$

Considering the discharge of the diffuser as incompressible flow with a sudden area enlargement:

$$\frac{\bar{P}_2 - \bar{P}_e}{\bar{q}_1} = \left(1 - \frac{A_2}{A_e}\right)\frac{\bar{q}_2}{\bar{q}_1} \tag{C7}$$

or

$$\frac{\bar{P}_2 - \bar{P}_e}{\bar{q}_1} = \left[1 - \left(\frac{A_2}{A_1}\right)\left(\frac{A_1}{A_e}\right)\right]\frac{\bar{q}_2}{\bar{q}_1} \tag{C8}$$

From equation (C2), for incompressible flow

$$\frac{\bar{q}_2}{\bar{q}_1} = \left(\frac{A_1}{A_2}\right)^2 \tag{C9}$$

Thus, equation (C8) becomes

$$\frac{\bar{P}_2 - \bar{P}_e}{\bar{q}_1} = \left[1 - \left(\frac{A_2}{A_1}\right)\left(\frac{A_1}{A_e}\right)\right]\left(\frac{A_1}{A_2}\right)^2 \tag{C10}$$

The desired overall total-pressure loss is obtained by the addition of equations (C5) and (C10).

$$\frac{\overline{P}_1 - \overline{P}_e}{\overline{q}_1} = \left[1 - \frac{1}{\left(\frac{A_2}{A_1}\right)^2}\right] + \frac{1}{\left(\frac{A_2}{A_1}\right)^2}\left[1 - \left(\frac{A_2}{A_1}\right)\left(\frac{A_1}{A_e}\right)\right] - \left(\frac{p_2 - p_1}{\overline{q}_1}\right) \tag{C11}$$

which can be simplified to

$$\frac{\overline{P}_1 - \overline{P}_e}{\overline{q}_1} = 1 - \frac{\frac{A_1}{A_e}}{\frac{A_2}{A_1}} - \frac{p_2 - p_1}{\overline{q}_1} \tag{C12}$$

The calculated variation of overall total-pressure-loss coefficient from equation (C12) is shown in figure 31, where the total-pressure-loss coefficient $(\overline{P}_1 - \overline{P}_e)/\overline{q}_1$ is plotted as a function of the area ratio. The curve shown corresponds to the values of maximum static-pressure recovery for each area ratio (fig. 30).

Figures 30 and 31 were used to select the design variable of included diffuser angle and area ratio. From figure 31 it can be seen that the total-pressure loss coefficient decreases significantly as area ratio is increased to approximately 3, after which the decrease become relatively small. Therefore, to minimize length, an area ratio of 2.9 was selected for the V/STOL diffuser, as shown on the curve. The predicted total-pressure-loss coefficient is about 0.195.

The predicted performance curve for a diffuser with an area ratio of 2.9 and $2\delta^*/D_1 = 0.01$ is shown by the dashed line in figure 30. The angle which corresponds to the maximum static-pressure recovery is 6.8°. With the inlet area equal to 36.7 square meters (137.25 ft^2) and the area ratio and diffuser included angle chosen as 2.9° and 6.8°, respectively, the diffuser length becomes 20.1 meters (68 ft). The diffuser exit dimensions are then 5.19 meters by 7.09 meters (17 by 23.25 ft).

REFERENCES

1. Pope, Alan; and Harper, John J.: Low-Speed Wind Tunnel Testing. John Wiley & Sons, Inc., 1966.
2. Schlichting, Hermann (J. Kestin, trans.): Boundary Layer Theory. Fourth ed., McGraw-Hill Book Co., Inc., 1960.
3. Staff of Lewis Laboratory: Central Automatic Data Processing System. NACA TN 4212, 1958.
4. Rouse, Hunter; and Hassan, M. M.: Cavitation-Free Inlets and Contractions. Mech. Eng., vol. 71, no. 3, Mar. 1949, pp. 213-216.
5. Heyson, Harry H.: Linearized Theory of Wind-Tunnel Jet-Boundary Corrections and Ground Effect for VTOL-STOL Aircraft. NASA TR R-124, 1962.
6. Lo, Ching-Fang; and Binion, Travis W., Jr.: A V/STOL Wind-Tunnel Wall Interference Study. J. Aircraft, vol. 7, no. 1, Jan.-Feb. 1970, pp. 51-57.
7. Garner, H. C., ed.: Subsonic Wind Tunnel Wall Corrections. AGARDograph 109, 1966.
8. Heyson, Harry H.: Use of Superposition in Digital Computers to Obtain Wind-Tunnel Interference Factors for Arbitrary Configurations, with Particular Reference to V/STOL Models. NASA TR R-302, 1969.
9. Joppa, Robert G.: A Method of Calculating Wind Tunnel Interference Factors of Arbitrary Cross-Section. NASA CR-845, 1967.
10. Grunwald, Kalman J.: Experimental Study of Wind-Tunnel Wall Effects and Wall Corrections for a General-Research V/STOL Tilt-Wing Model with Flap. NASA TN D-2887, 1965.
11. Davenport, Edwin E.; and Kuhn, Richard E.: Wind-Tunnel-Wall Effects and Scale Effects on a VTOL Configuration with a Fan Mounted in the Fuselage. NASA TN D-2560, 1965.
12. Reneau, L. R.; Johnston, J. P.; and Kline, S. J.: Performance and Design of Straight, Two-Dimensional Diffusers. Rep. PD-8, Standford Univ., Dept. Mech. Eng., Sept. 1964.
13. Henry, John R.; Wood, Charles C.; and Wilbur, Stafford W.: Summary of Subsonic-Diffuser Data. NACA RM L56F05, 1956.

TABLE I. - PATCH PANEL CONNECTORS

Quantity	Type	Cable type
55	MS3102-20-21S	One pair; individual shield; number 20 gage wire
24	Marlin Mfg. Co. number 1061K	Thermocouple; single pair; Chromel-Alumel number 20 gage wire
3	Bendix Corp. PTO2W-B-3P	One pair; shielded; number 20 gage wire
1	Microdot, Inc., number 033-0055	Coaxial; Microdot, Inc.; number 293-3920

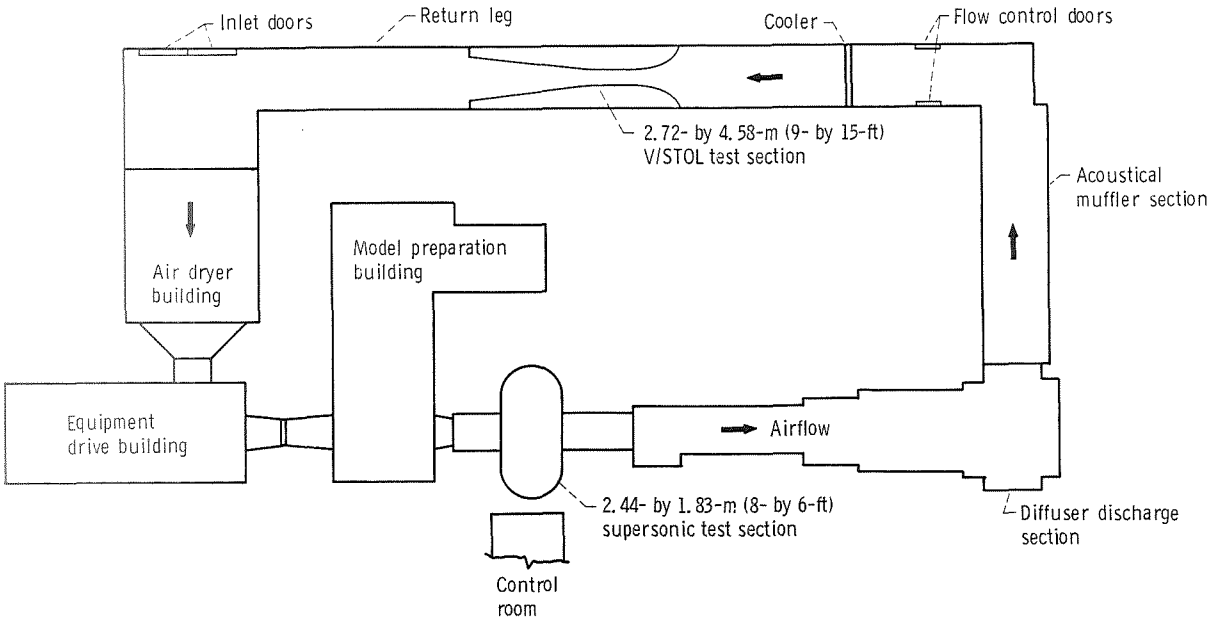

Figure 1. - Overall plan view of V/STOL test facility in the return leg of the 8- by 6-Foot Supersonic Wind Tunnel.

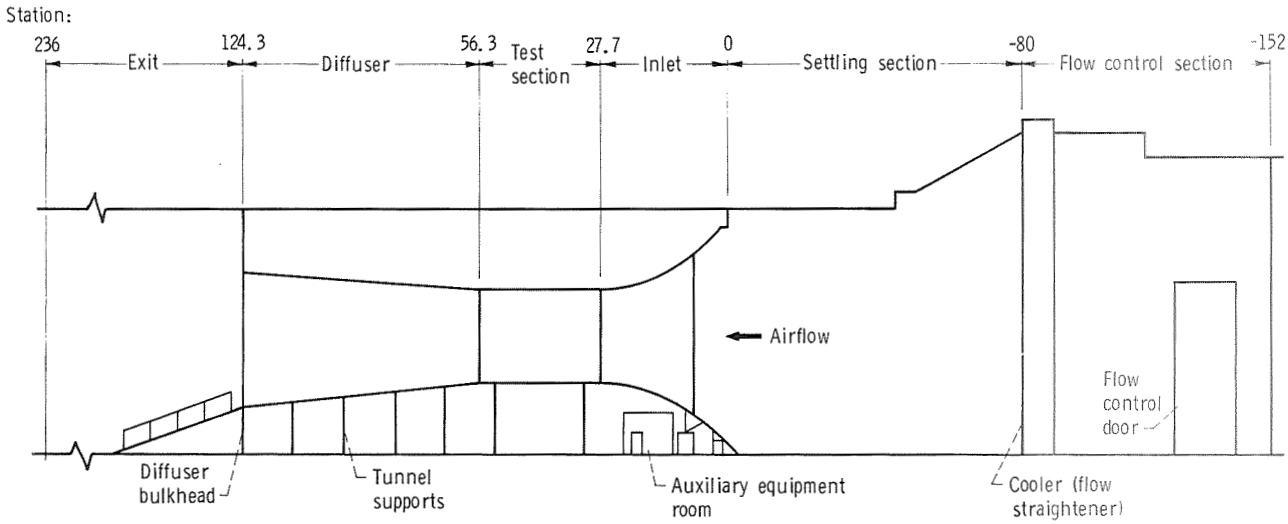

Figure 2. - Schematic elevation view of 2.72- by 4.58-meter (9- by 15-ft) V/STOL facility. (Drawing not to scale.)

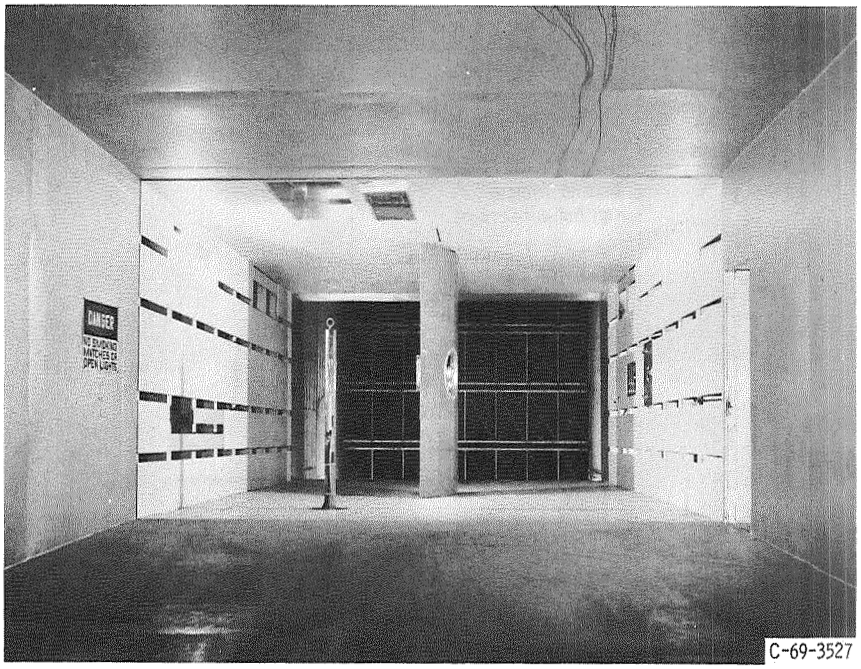

Figure 3. - Test-section wall slot configuration.

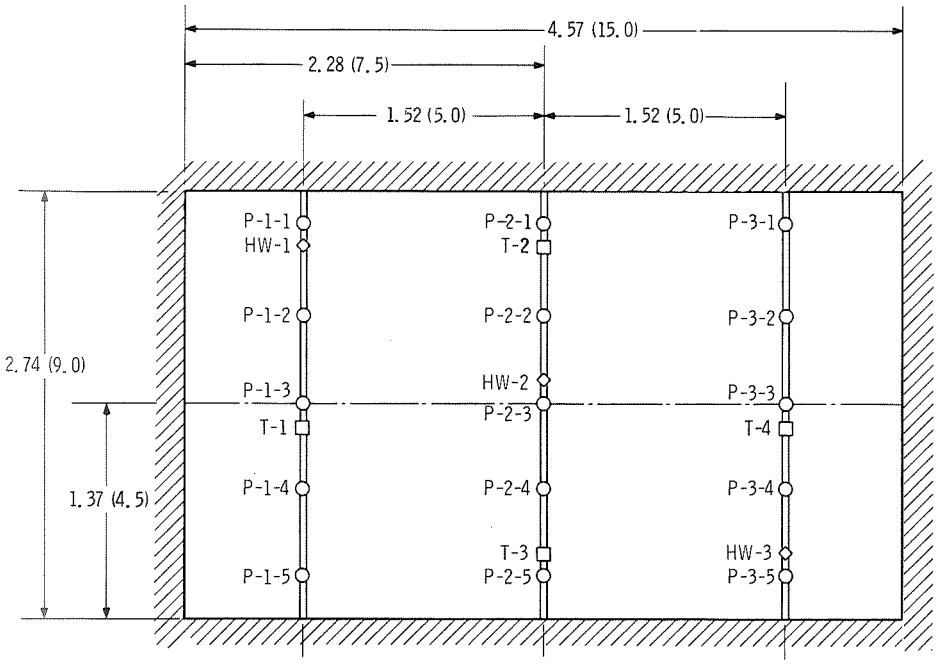

(a) Elevation view of V/STOL test section looking downstream.

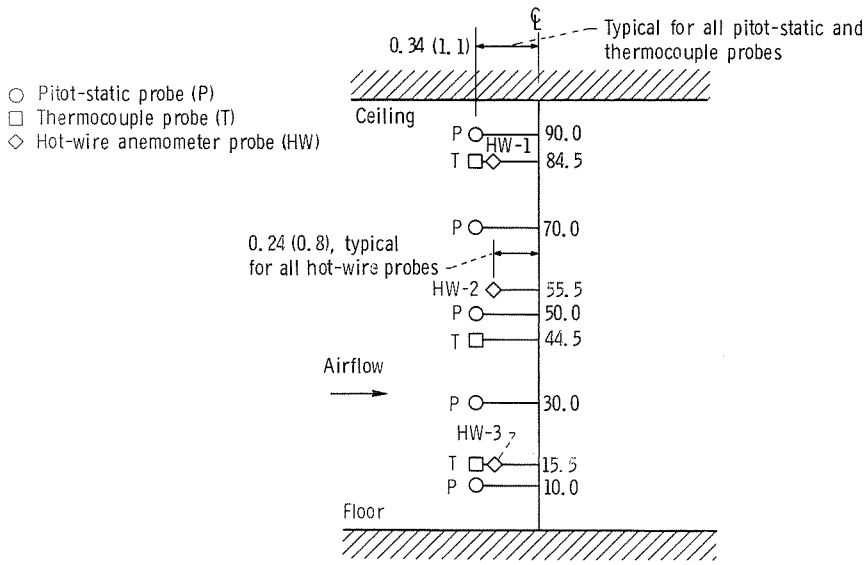

(b) Probe elevations in percent of tunnel height from floor.

Figure 4. - Calibration probe locations. Unless otherwise noted, all dimensions are in meters (ft).

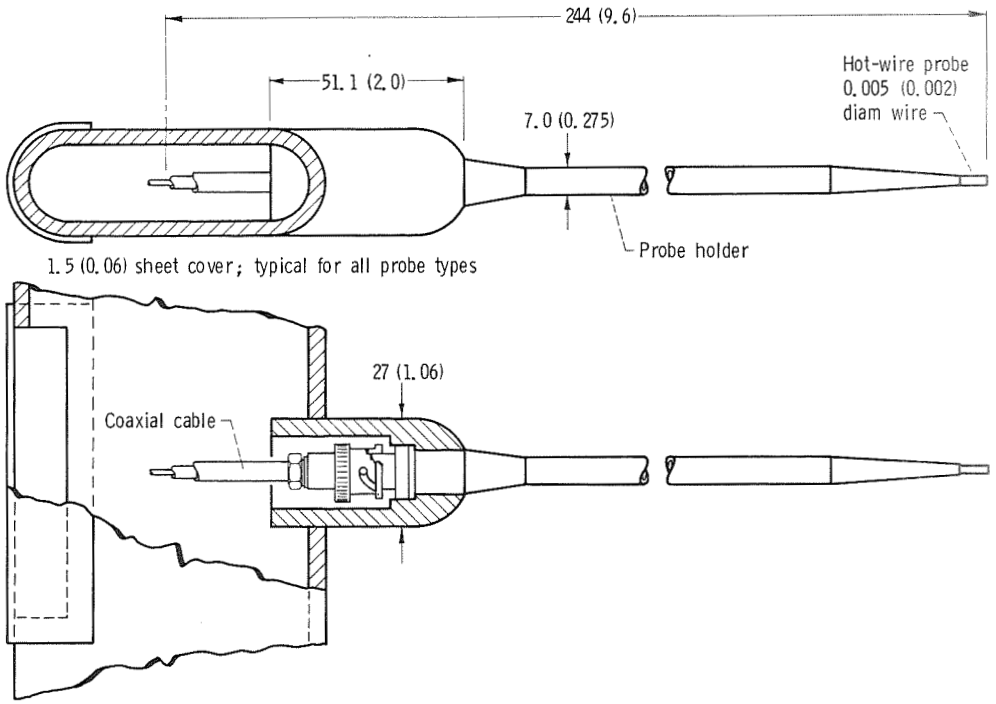

(a) Hot-wire probe.

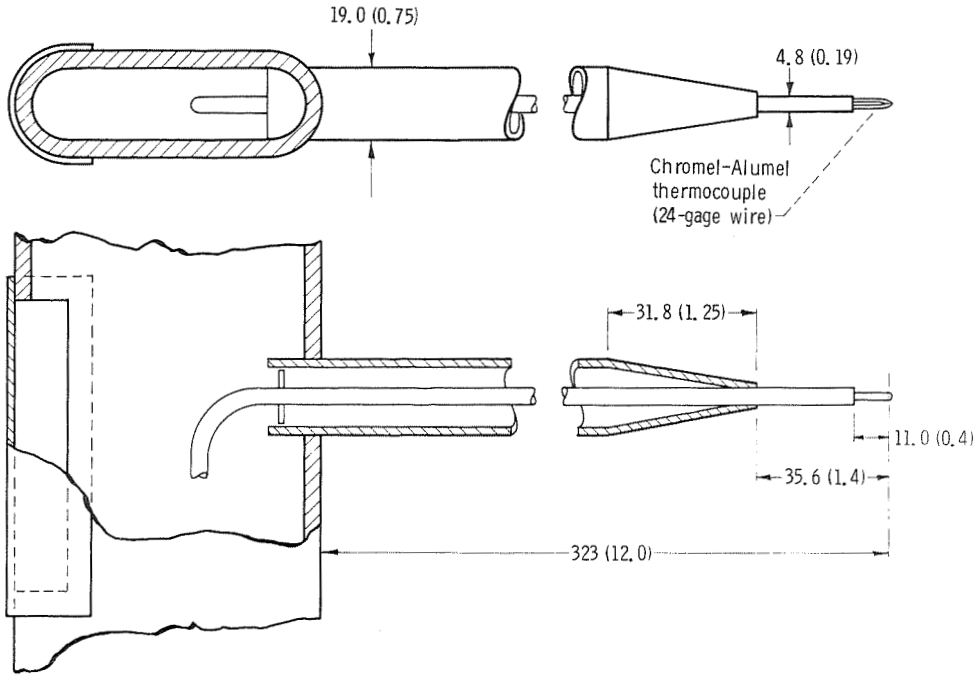

(b) Temperature probe.

Figure 5. - Probe details. All dimensions are in millimeters (in.) unless noted otherwise.

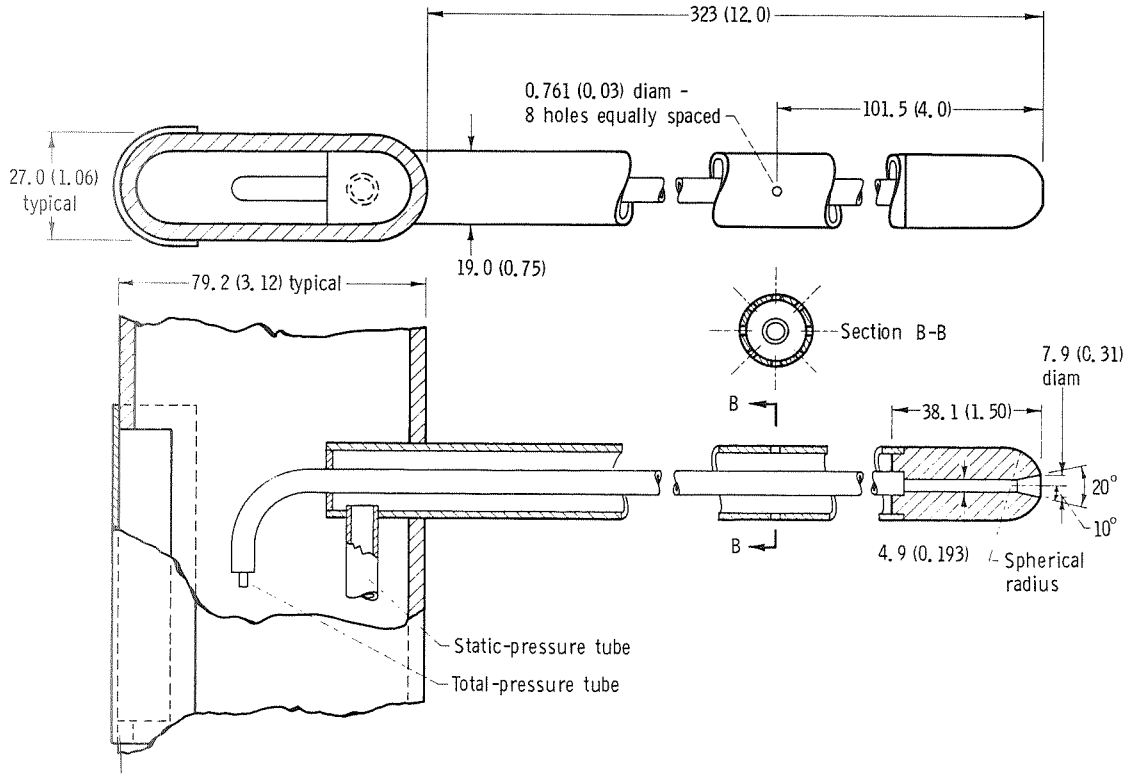

(c) Pitot-static probe.

Figure 5. - Concluded.

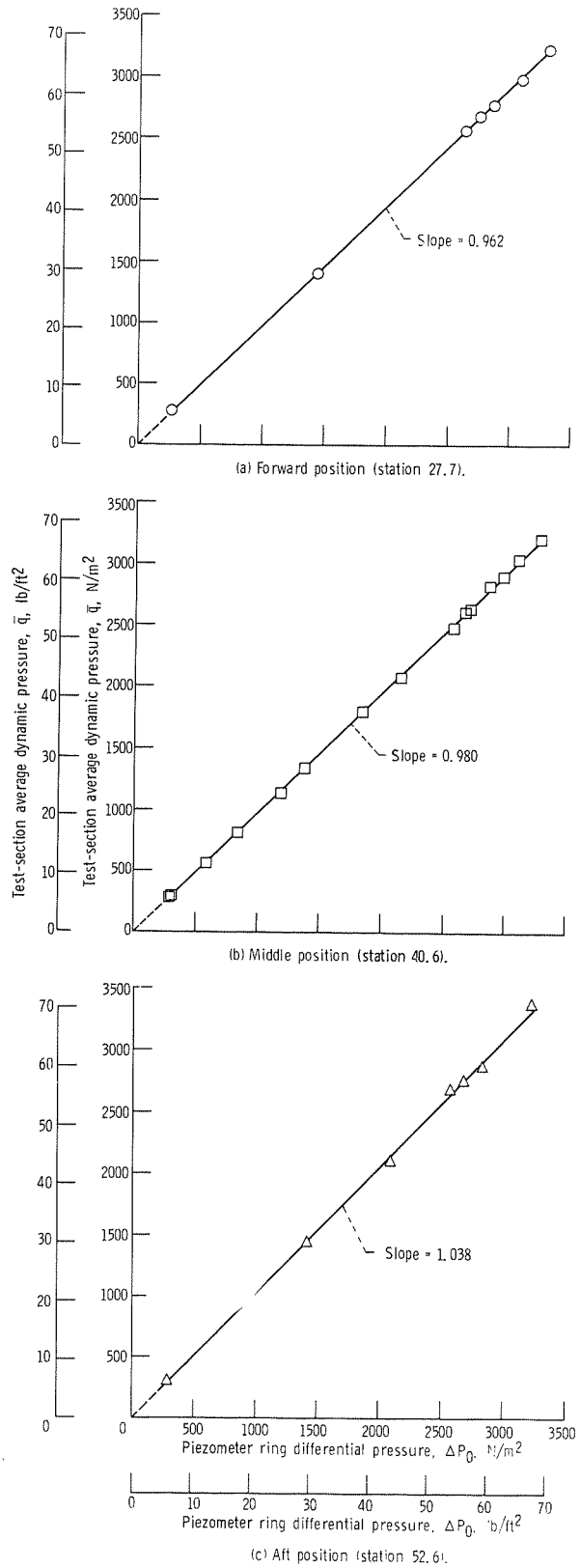

Figure 6. - Correlation of piezometer ring differential pressure and test-section dynamic pressure.

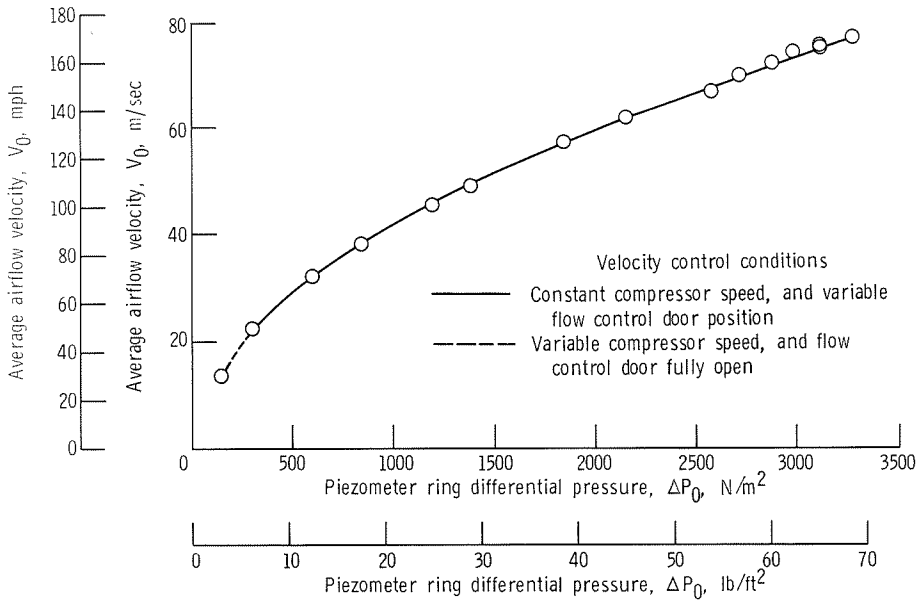

Figure 7. - V/STOL test-section velocity range at midposition. Tunnel total temperature, 303 K (545° R).

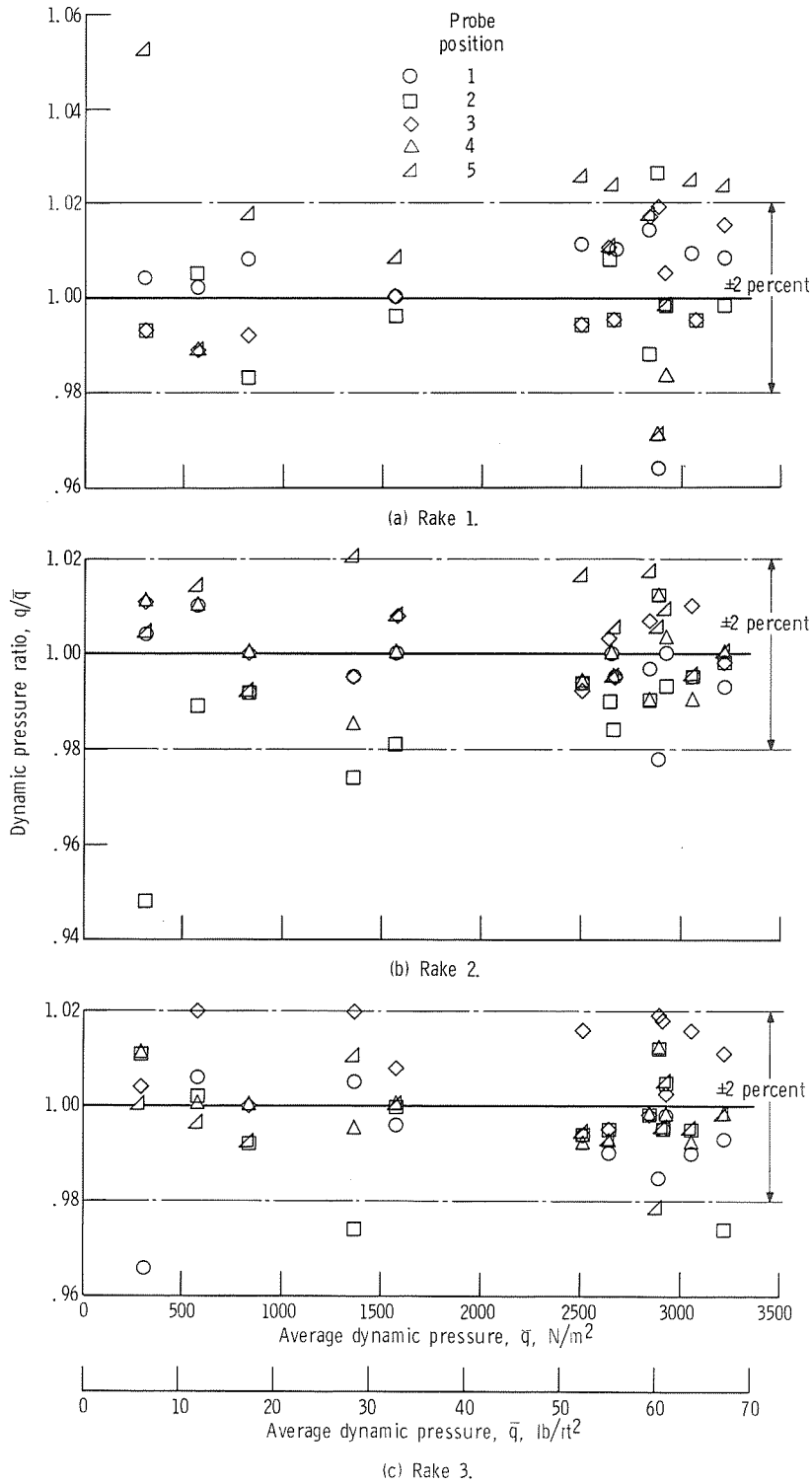

(a) Rake 1.

(b) Rake 2.

(c) Rake 3.

Figure 8. - Test-section dynamic pressure variation at midposition (station 40.6).

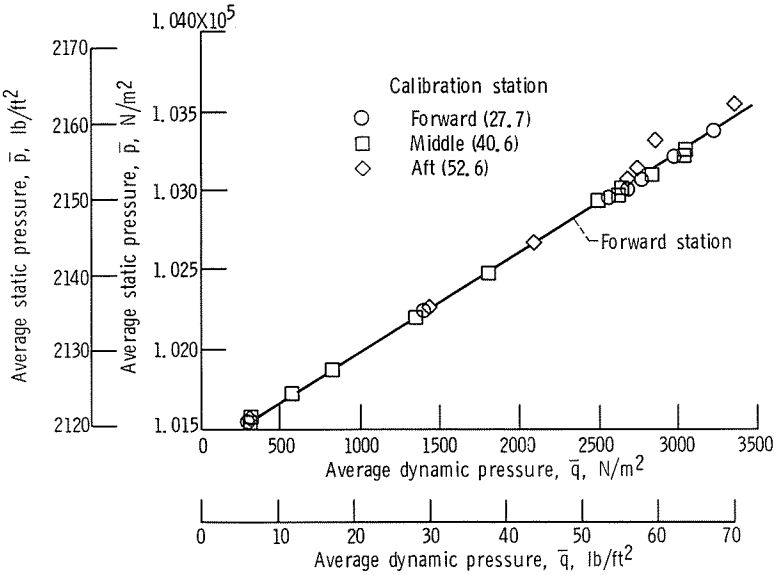

Figure 9. - Test-section static-pressure variation.

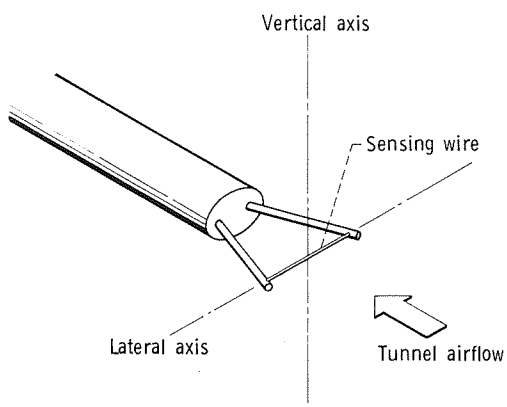

Figure 10. - Orientation of hot-wire probe in tunnel airflow.

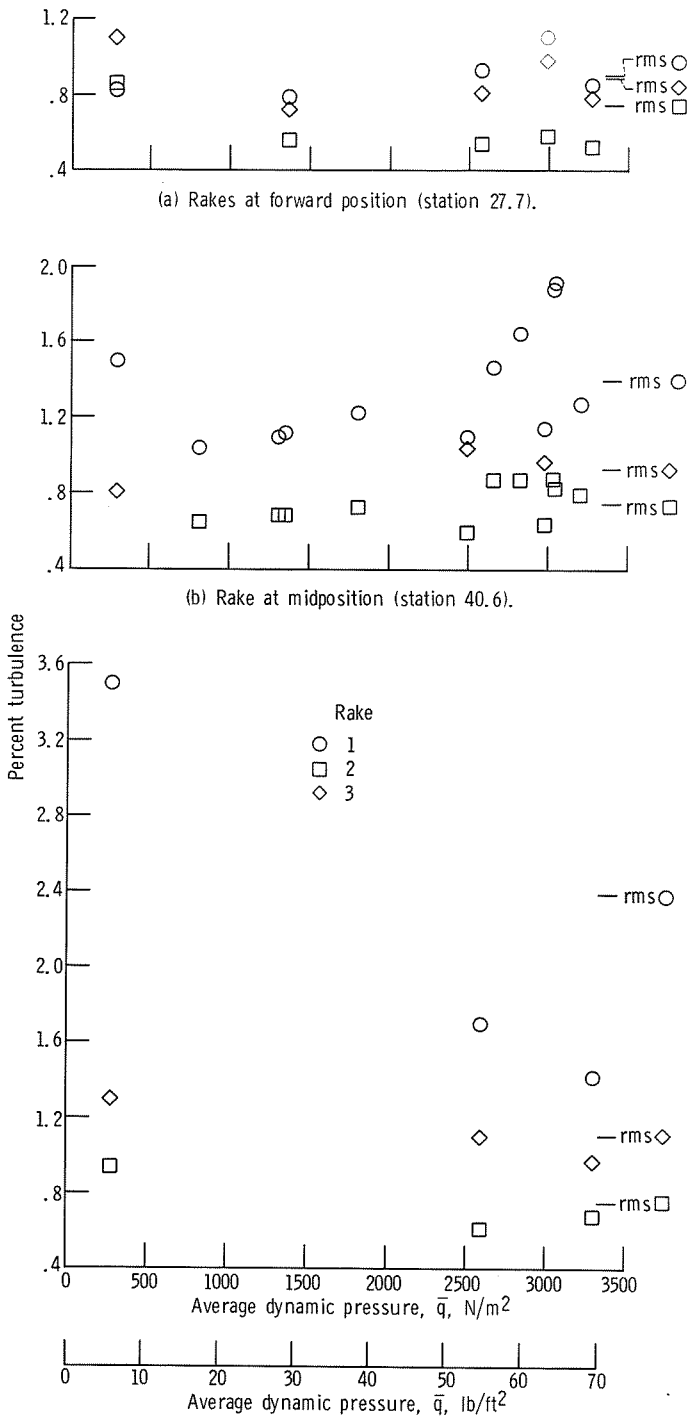

(a) Rakes at forward position (station 27.7).

(b) Rake at midposition (station 40.6).

(c) Rake at aft position (station 52.6).

Figure 11. - Percent turbulence in test section with 40-percent-open slotted walls.

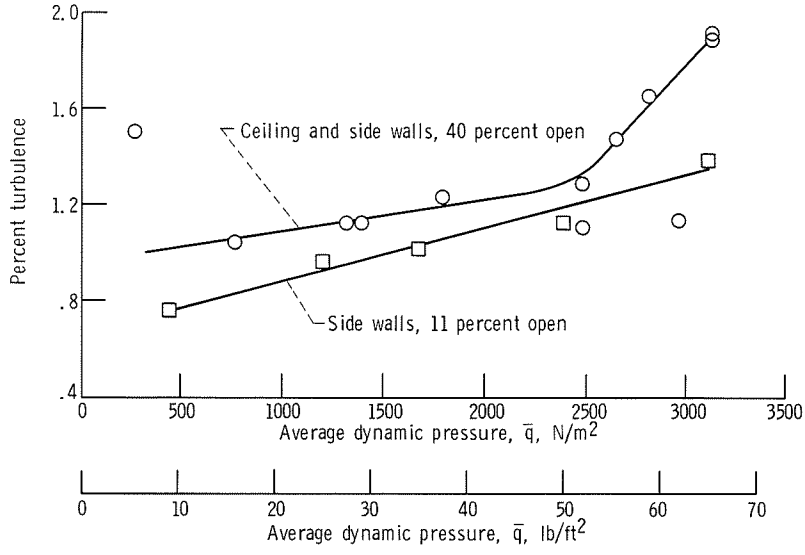

Figure 12. - Turbulence level on rake 1 at midposition (station 40.6) with two wall slot configurations.

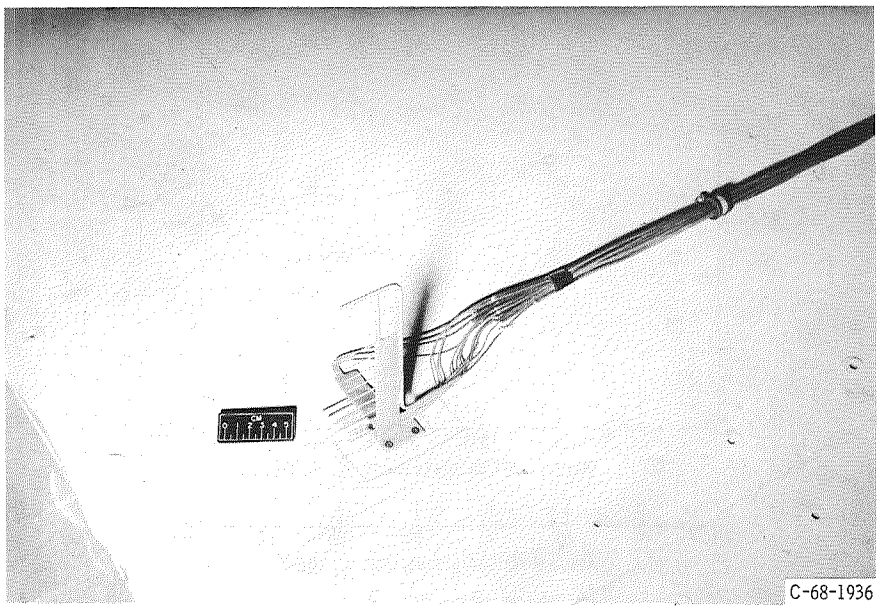

Figure 13. - Boundary-layer rake.

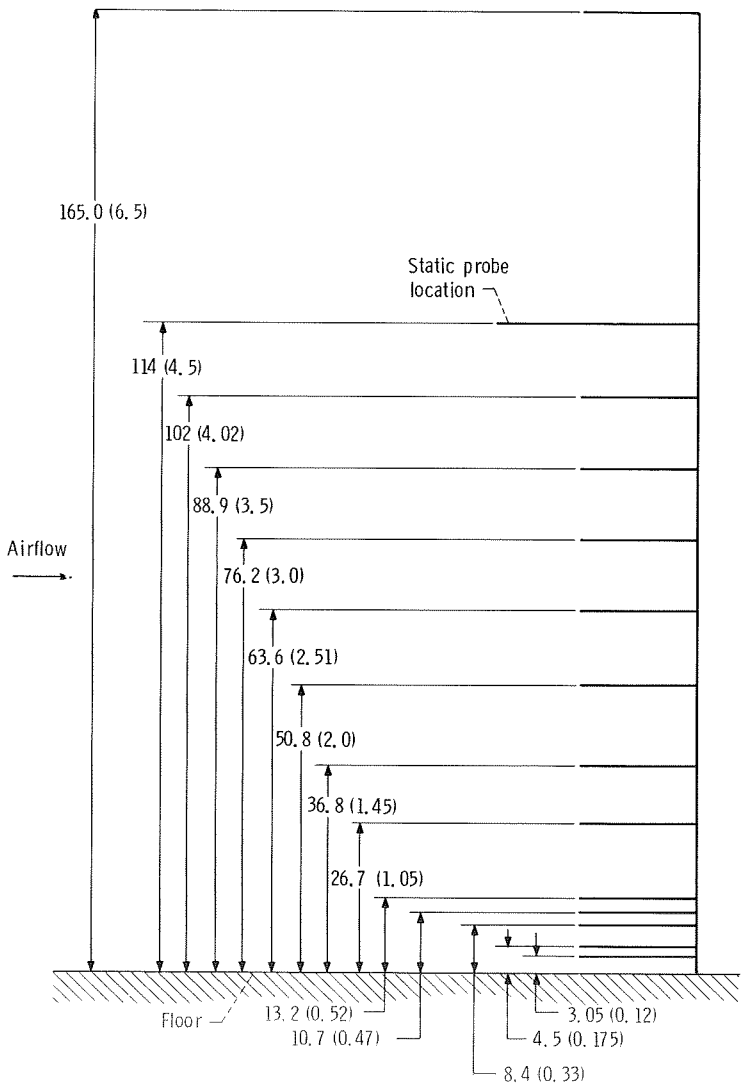

Figure 14. - Boundary-layer rake probe locations. (All dimensions are in millimeters (in.).)

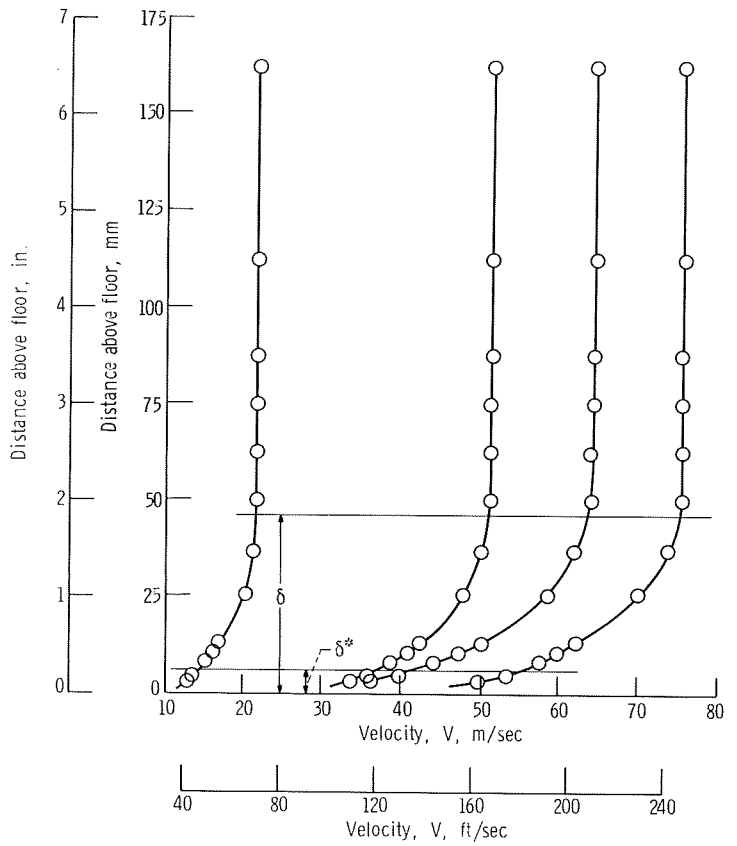

Figure 15. - Boundary-layer profiles 158 millimeters (6.2 in.) downstream of the entrance to the test section.

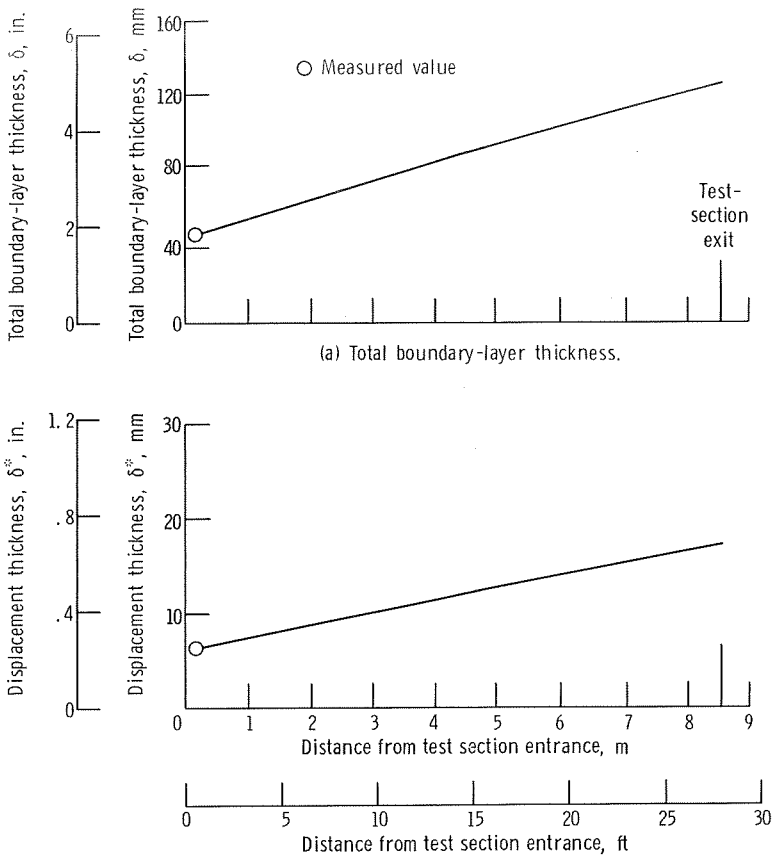

(a) Total boundary-layer thickness.

(b) Displacement thickness.

Figure 16. - Estimated boundary-layer thickness on tunnel floor.

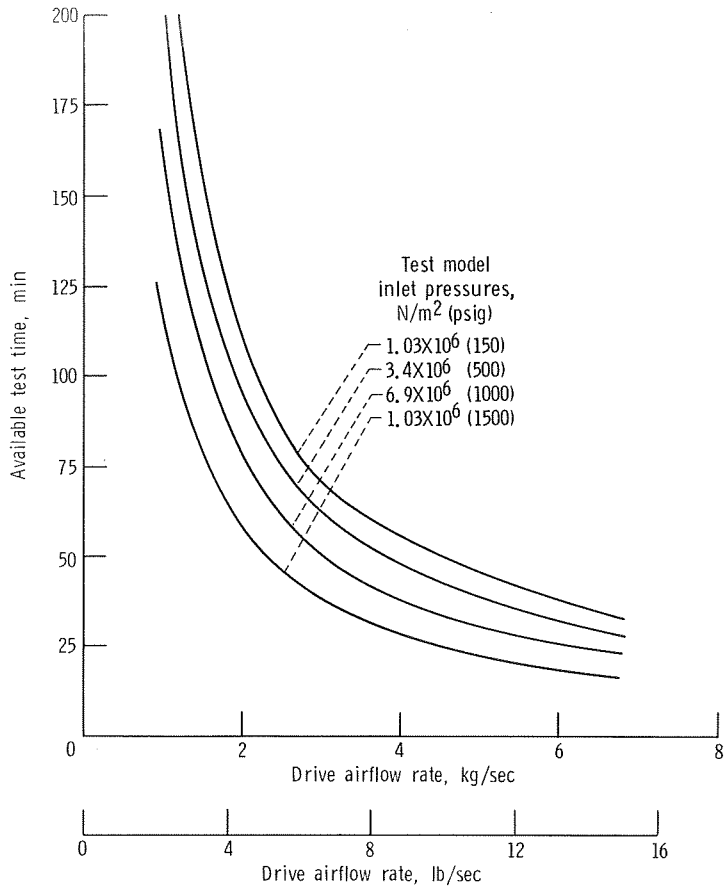

Figure 17. - Available test time as function of test model flow rate and pressure level.

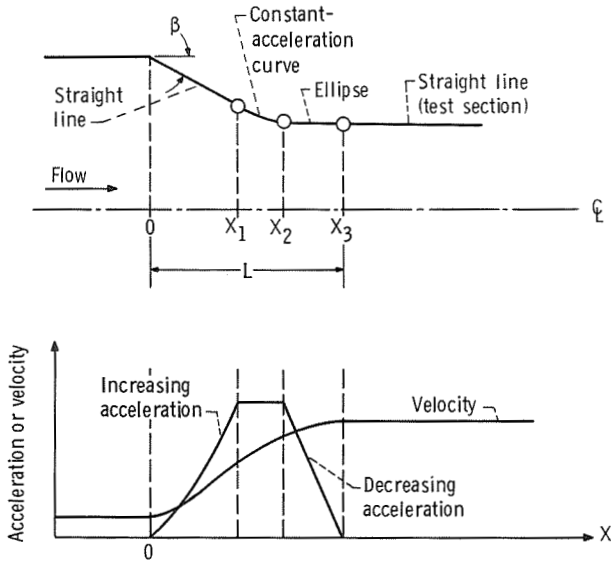

Figure 18. - Modified constant-acceleration tunnel inlet wall contour.

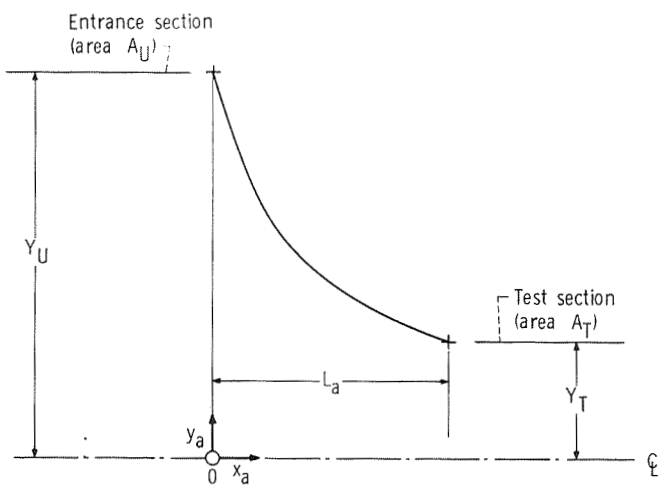

Figure 19. - Constant-acceleration curve over length L_a.

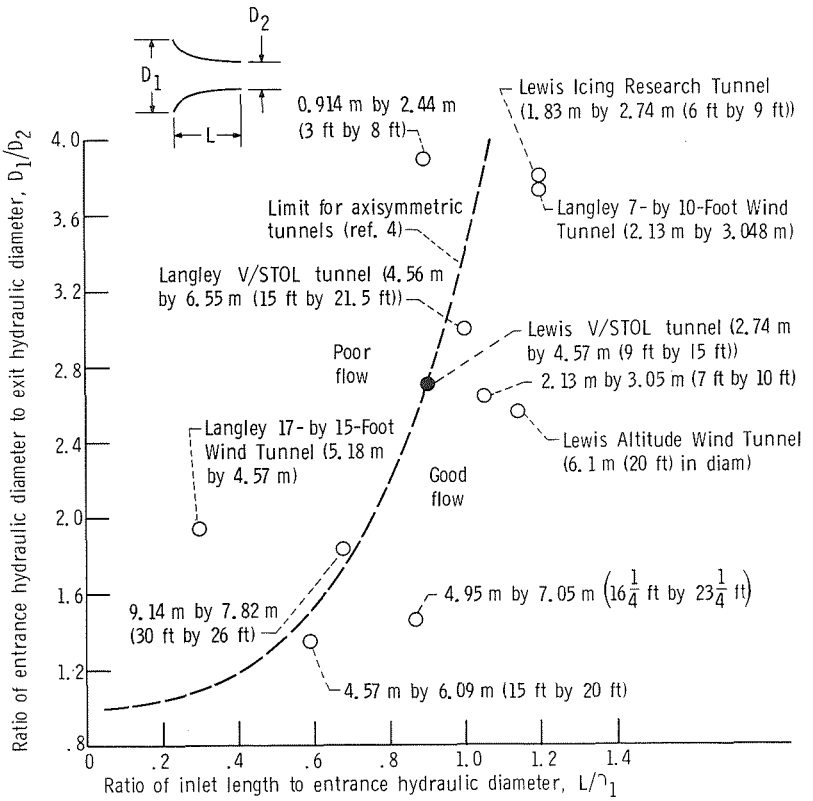

Figure 20. - Inlet section design limits. (Dimensions are those of wind tunnel test section in meters (ft). The location of nongovernment facilities is not specified.)

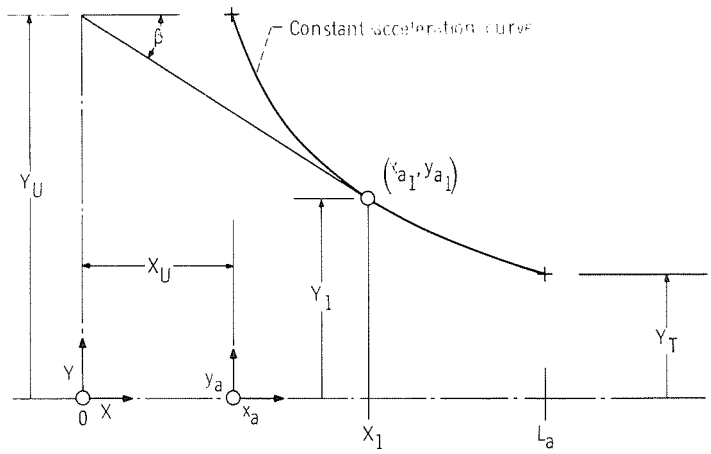

Figure 21. - Straight-line-section geometry.

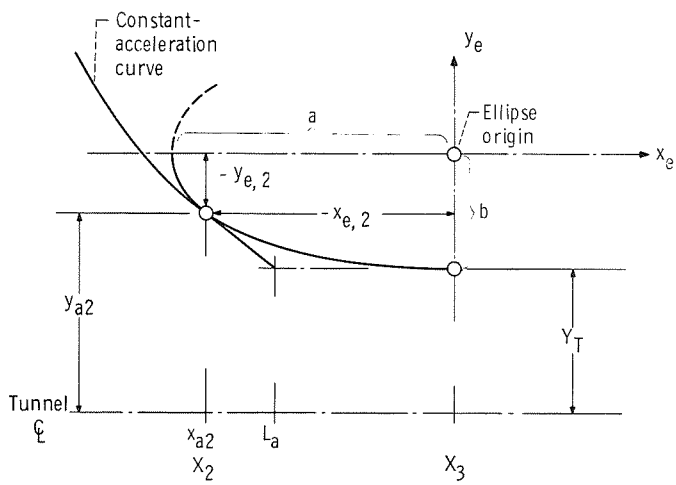

Figure 22. - Ellipse geometry.

	Ordinates of inlet			
	Side walls		Top and bottom walls	
	m	ft	m	ft
Y_1	1.939	6.361	2.853	9.361
Y_2	1.299	5.903	2.714	8.903
Y_3	1.687	5.535	2.602	8.535
Y_4	1.599	5.247	2.514	8.247
Y_5	1.528	5.012	2.442	8.012
Y_6	1.516	4.934	2.430	7.934
Y_7	1.468	4.816	2.382	7.816
Y_8	1.435	4.707	2.349	7.707
Y_9	1.410	4.627	2.325	7.627
Y_{10}	1.393	4.569	2.307	7.569
Y_{11}	1.381	4.530	2.295	7.530
Y_{12}	1.374	4.507	2.289	7.507
Y_{13}	1.372	4.500	2.286	7.500

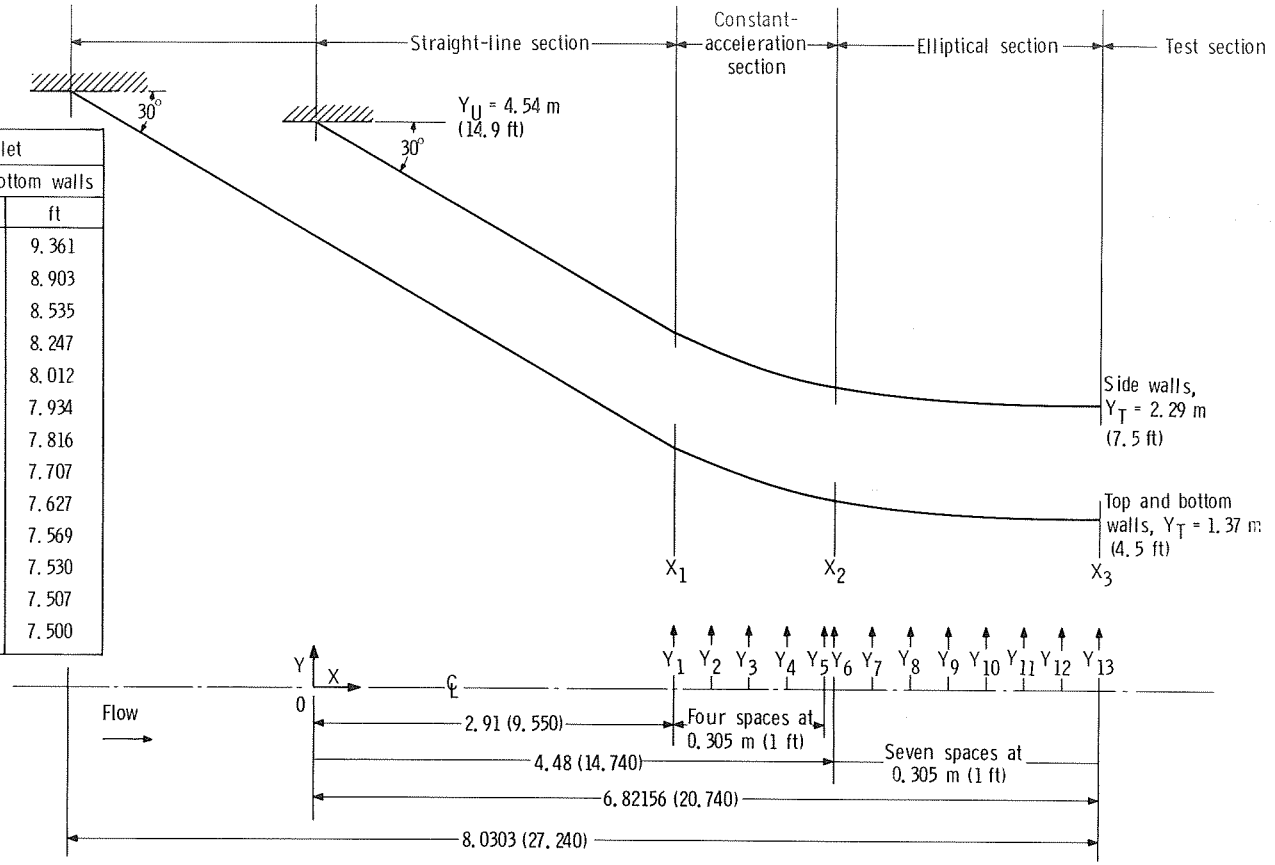

Figure 23. - Design coordinates for V/STOL inlet contraction section. (Dimensions are in meters (ft).)

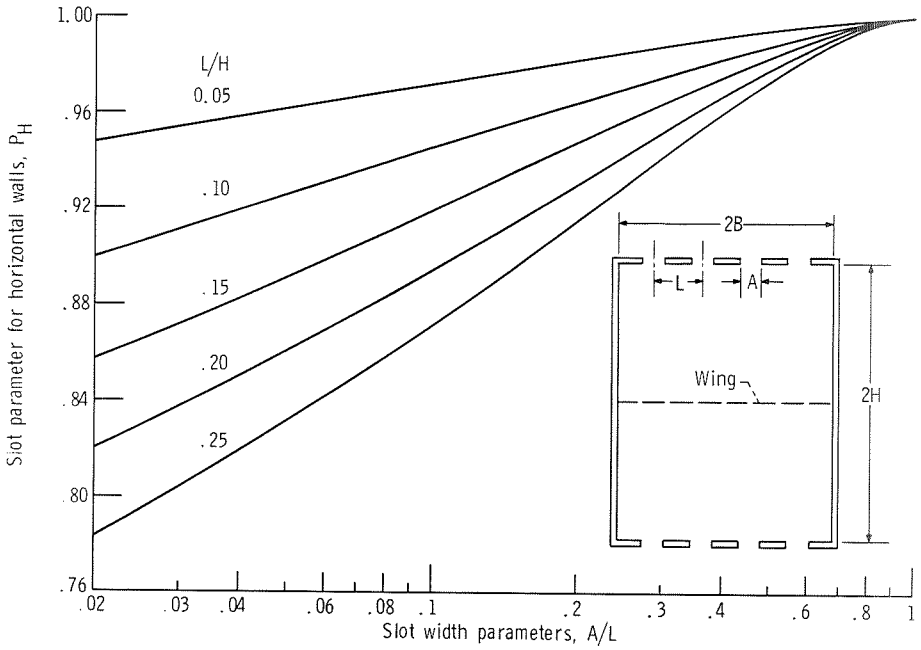

Figure 24. - Slot geometry parameters. (From ref. 6.)

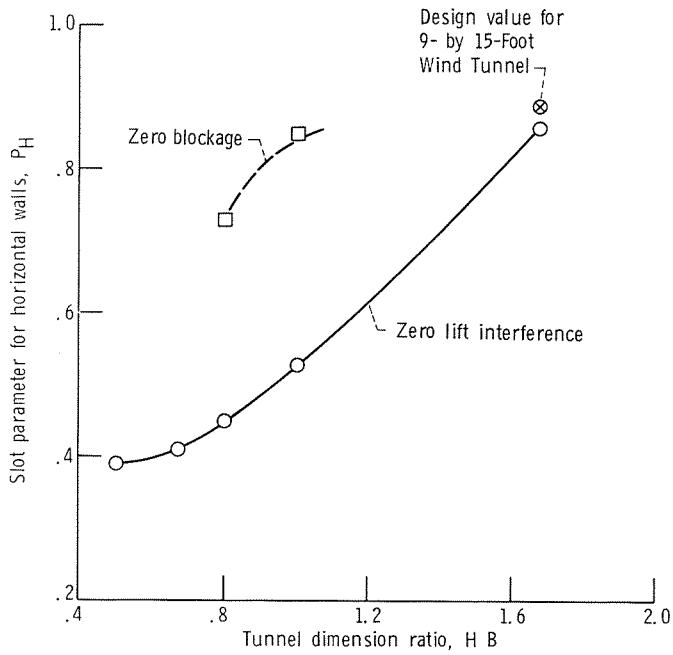

Figure 25. - Slot parameters for zero lift interference for a wind tunnel with closed vertical walls. Slot parameter for vertical walls, $P_V = 0$. (From ref. 5.)

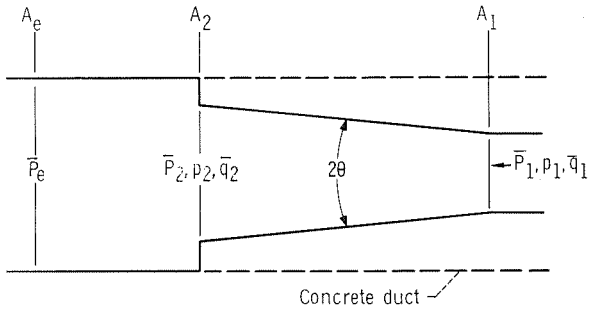

Figure 26. - V/STOL tunnel diffuser configuration.

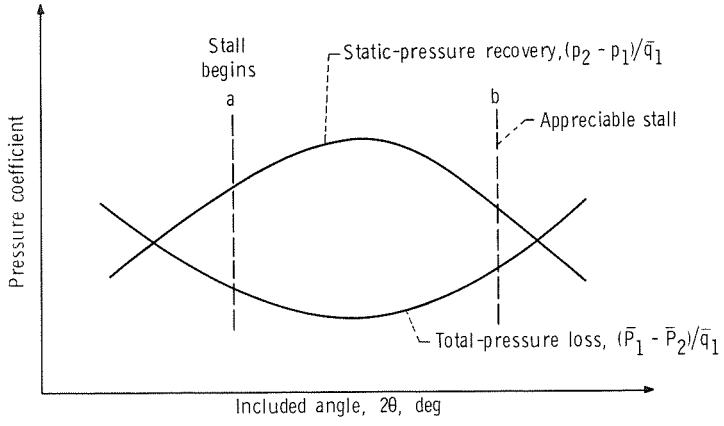

Figure 27. - Typical diffuser performance curve for fixed area ratio and inlet boundary-layer thickness.

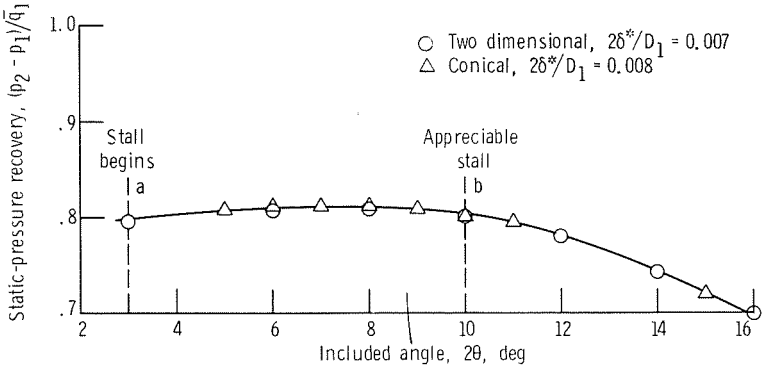

Figure 28. - Comparison of diffuser static-pressure recovery for an area ratio, $A_2/A_1 = 3.0$. (Data from refs. 12 and 13.)

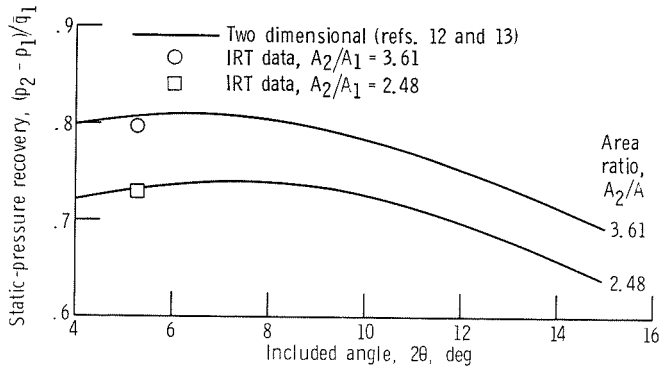

Figure 29. - Comparison of predicted and measured static-pressure recovery for two axial locations in Icing Research Tunnel (IRT) diffuser ($2\delta^*/D_1$ = 0.01).

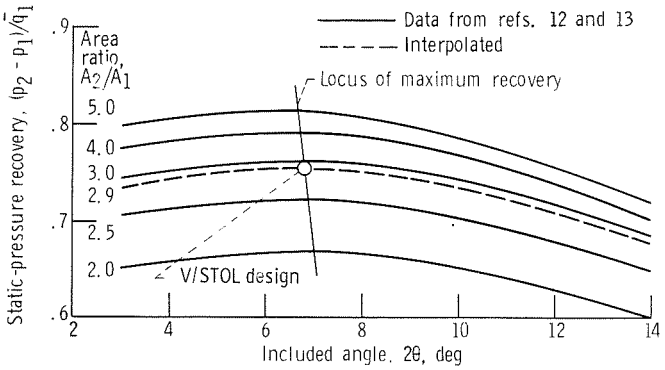

Figure 30. - Diffuser performance curves for boundary-layer thickness parameter $2\delta^*/D_1 \approx 0.01$.

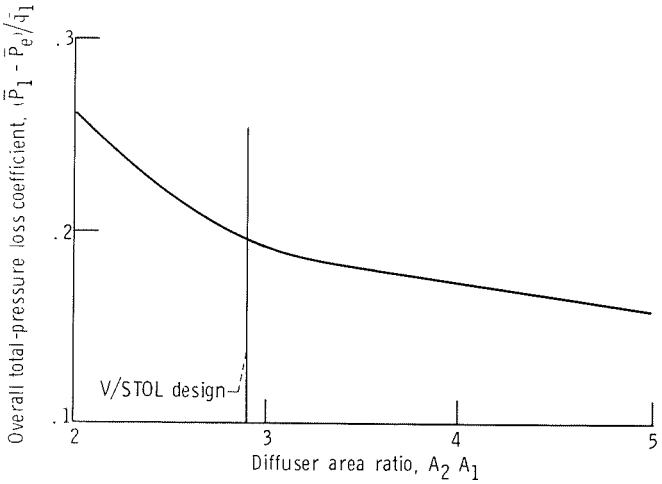

Figure 31. - Calculated overall total-pressure loss for diffuser with sudden expansion. Determined at maximum static-pressure recovery and for boundary-layer thickness parameter $2\delta^*/D_1 \approx 0.01$. Area ratio, A_1/A_e = 0.141.

NATIONAL AERONAUTICS AND SPACE ADMINISTRATION
WASHINGTON, D. C. 20546

OFFICIAL BUSINESS
PENALTY FOR PRIVATE USE $300

FIRST CLASS MAIL

POSTAGE AND FEES PAID
NATIONAL AERONAUTICS AND
SPACE ADMINISTRATION

POSTMASTER: If Undeliverable (Section 158 Postal Manual) Do Not Return

"The aeronautical and space activities of the United States shall be conducted so as to contribute . . . to the expansion of human knowledge of phenomena in the atmosphere and space. The Administration shall provide for the widest practicable and appropriate dissemination of information concerning its activities and the results thereof."

— NATIONAL AERONAUTICS AND SPACE ACT OF 1958

NASA SCIENTIFIC AND TECHNICAL PUBLICATIONS

TECHNICAL REPORTS: Scientific and technical information considered important, complete, and a lasting contribution to existing knowledge.

TECHNICAL NOTES: Information less broad in scope but nevertheless of importance as a contribution to existing knowledge.

TECHNICAL MEMORANDUMS: Information receiving limited distribution because of preliminary data, security classification, or other reasons.

CONTRACTOR REPORTS: Scientific and technical information generated under a NASA contract or grant and considered an important contribution to existing knowledge.

TECHNICAL TRANSLATIONS: Information published in a foreign language considered to merit NASA distribution in English.

SPECIAL PUBLICATIONS: Information derived from or of value to NASA activities. Publications include conference proceedings, monographs, data compilations, handbooks, sourcebooks, and special bibliographies.

TECHNOLOGY UTILIZATION PUBLICATIONS: Information on technology used by NASA that may be of particular interest in commercial and other non-aerospace applications. Publications include Tech Briefs, Technology Utilization Reports and Technology Surveys.

Details on the availability of these publications may be obtained from:

SCIENTIFIC AND TECHNICAL INFORMATION OFFICE

NATIONAL AERONAUTICS AND SPACE ADMINISTRATION

Washington, D.C. 20546